Understanding energy transfer in aeroelastic flutter and exploiting free-play induced flutter for energy harvesting

by

Prachi Deepak Deshpande

A thesis submitted to the graduate faculty

in partial fulfillment of the requirements for the degree of

MASTER OF SCIENCE

Major: Mechanical Engineering

Program of Study Committee:

Atul Kelkar, Major Professor

Partha Sarkar

Ming-Chen Hsu

Iowa State University

Ames, Iowa

2016

DEDICATION

I would like to dedicate this thesis to my father Deepak and mother Aparna. Their unending support, encouragement and motivation is the most integral part of the whole journey.

TABLE OF CONTENTS

LIST OF TABLES

LIST OF FIGURES

ACKNOWLEDGEMENTS

I would like to take this opportunity to express my heartfelt gratitude to all people who helped me with various aspects of my masters program, conducting research and the writing of this thesis.

First and foremost, I thank my advisor Dr. Atul Kelkar for his generous support, advices, patience and continuous guidance at each and every step. He was very helpful throughout my graduate program, research and the writing of this thesis. I greatly appreciate VSI Aerospace, Inc., Ames, IA for sharing the data useful for this work.

I would also like to thank my committee members for their efforts, insights and contributions to this work. Dr. Ming-Chen Hsu and his group was really helpful whenever needed during the project work. I am thankful to Dr. Sarkar for his guidance in the graduate program and this work. Also, I am grateful to Dr. Dayal for his time and suggestions whenever required.

I extend my thanks to the Department of Mechanical Engineering for financial assistance and all the support they provided throughout my graduate program.

I express my gratitude to my friends for their guidance, motivation, useful discussions and confidence on me. My deepest thanks to my family, without their continuous encouragement and unending support it was impossible for me to reach here. They are the strong pillars of my foundation.

ABSTRACT

Aeroelasticity is well established research area involving undesirable coupling between elasticity, inertia and aerodynamics. Flutter is characterized as an unstable self excited aeroelastic system response, which leads to catastrophic structural failure. It is widely studied how various nonlinearities in fluid flow, structural stiffness, damping, and free-play in the joints affect the phenomenon in different ways. While most of the work in the literature is focused on how to avoid potentially catastrophic onset of flutter, this work unravels the mechanism of energy exchange that takes place between coupled fluid and structure system. The focus of this work is to investigate how to harness the energy in otherwise undesirable phenomenon. The flutter state of interest is the limit cycle oscillations(LCO) which represents marginally stable structural response. More fundamental study aimed at energy aspect of the interaction is done using a simple 2D airfoil (NACA 0012) system with two degrees of freedom and hyperbolic free-play nonlinearity. Variation of kinetic, potential, total energy and balanced energy interaction are established and analyzed in details. The representative experimental results are discussed from energy perspective which motivated the development of high fidelity fully coupled computational model discussed in this thesis. The work presents energy transfer dynamics for this 3D model. The energy analysis from 2D and 3D configuration suggests that there is a potential for harnessing energy that is transferred from flow field to the structure during aeroelastic flutter. The magnetostrictive materials like Galfenol can be used to efficiently convert the energy transferred to the structure by flow field into electrical energy. The dynamics of magnetostriction for Galfenol is presented using published properties of Galfenol by its manufacturer Etrema. For an example, 3D airfoil system simulation results are presented for open circuit voltage that will be generated using the proposed concept. This research gives a deeper understanding of energy exchange between structure and flow field during different phases of dynamic response of aeroelastic system.

CHAPTER 1.   INTRODUCTION

1.1   Background Review

1.1.1   Aeroelasticity and Flutter

Aeroelasticity deals with interaction of fluid and structure dynamics when an elastic structure is kept in the fluid flow. Its a well researched field and there has been a high research interest in modelling and understanding the nonlinear dynamics involved in this [Ko et al. (1997), Ko et al. (1998), Trickey et al. (2002), Northington (2009)]. The study of aeroelasticity and its control involve many diverse disciplines and deals with problems such as wing flutter, buffeting, divergence, control surface ineffectiveness-reversal etc. Figure 1.1 shows different aspects of aeroelasticity. Among these, flutter is the most feared dynamic instability. Many sudden structural failures due to aeroelasticy in the past have drawn researcher's attention to this subject and plethora of literature is available studying the various aspects of aeroelasticity, flutter, bifurcation analysis and modelling techniques associated with aeroelastic response. Flutter is self feeding undesirable system vibrations leading to catastrophic structural failures. Divergence is a static instability, where excessive aerodynamic forces caused by elastic deformation lead to structural failure. The static and dynamic influence along with steady or unsteady aerodynamics can also lead to undesirable conditions.

The topic of aeroelasticity has been addressed in many classic texts such as Earl H. Dowell and Sisto (1995), Theodorsen (1949) , Mukhopadhyay (2003) Edwards and Wieseman (2008). Due to nonlinear nature of the aeroelastic dynamics, these oscillations can be stable, bounded or divergent. Bounded oscillations are called limit cycle oscillations (LCO)whose magnitude is bounded but certainly dependent on the nature of nonlinearity. Many different techniques as given in Trickey (2000), Strganac et al. (2012), Lee et al. (1997), Lee et al. (1999) are used to
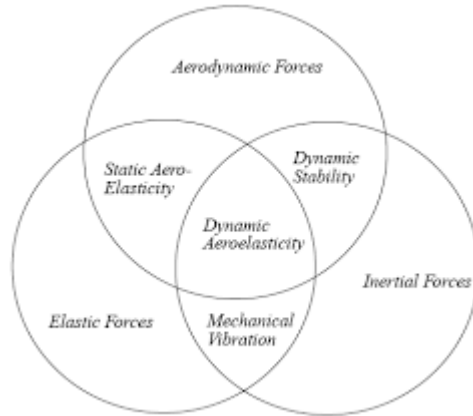
Figure 1.1   Aspects of Aeroelasticity

model various key parameters affecting the stability of the structure subsystem. These mainly include but not limited to nonlinearities in stiffness, damping, free-play in joints and inflow conditions. Typically, small nonlinear effects are removed by assuming linear behaviour at some operating points and restricting to the model to suitably small region about that point. Linearity is assumed in static or dynamic modelling to make the analysis simpler.

1.1.2   Free-play Nonlinearity

For an airfoil designed to rotate about a hinge line perpendicular to the free stream velocity, one of the most common structural nonlinearity is free-play in the rotational joints. Free-play in control surface is a range of rotation during which control surfaces move freely without any resistance. It is similar to backlash in gears. The continued wear and tear causes free-play to increase and eventually exceeds the maximum limit set during certification. Impact of free-play on flutter speed and frequency is not fully understood and hence very conservative estimates have been used for allowable free-play leading to stringent constraints. Hence, it becomes important to see how flutter is affected by free-play present in the rotational joint and assess its impact on aeroelastic response for better design approaches and manufacturing constraints [Tang and Dowell (2006), De-Min and Qi-Chang (2010), Trickey (2000)]. Specifically in the context of lifting airfoils such as wings, tails and control surfaces mounted on them, free-

play is a primary contributor to the LCO and diverging behaviour. Under the correct set of parameters, LCO is a bounded state but even if not divergent, it can significantly accelerate the fatigue of the structure leading to sudden failures. Early work done on in 1950s showed connection of free-play to flutter velocity but not until recently when a more in-depth analysis with experimental validation was performed to uncover the underlying dynamics explaining the dependence of flutter velocity on the size of the free-play. Studies mentioned in Whitmer et al. (2012), Asjes et al. (2014) have shown that rotational free-play lowers the flutter onset velocity and typically induces LCO mode of flutter.

1.1.3 Background

The work presented in this thesis is built on the previous work in Asjes (2015), Asjes et al. (2014) and Whitmer et al. (2012) on free- play nonlinearity modelling and its theoretical-experimental study of how flutter is affected by free-play. This work gives a systematic approach to characterize free-play effects for an accurate prediction of stability and performance boundaries. In this process, a modelling framework is developed to predict the dependence of flutter on free-play parameters. Simple 2D airfoil system with free-play nonlinearity is modelled as a feedback interconnection between linear system and sector bounded nonlinearity as shown in figure 1.2.
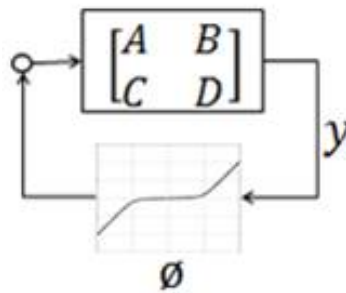

Figure 1.2   System with nonlinearity in feedback interconnection

Free-play nonlinearity affects stiffness behaviour about origin so a physically consistent free-play model requires stiffness to saturate close to a linear spring stiffness outside the free-
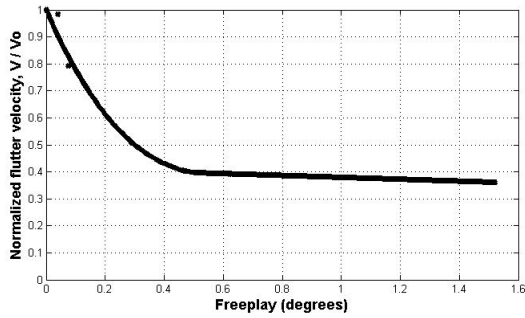
Figure 1.3   Flutter Velocity vs Free-play *
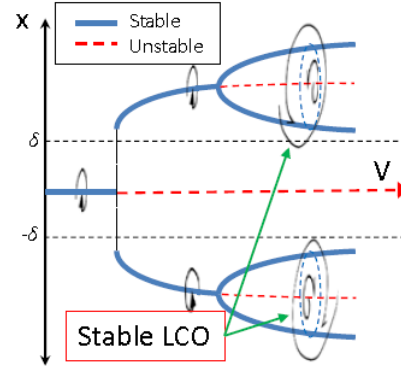
Figure 1.4   Hopf Bifurcation *

play region. Many candidate functions are studied in Asjes (2015), Asjes et al. (2014) and based on that free-play nonlinearity is modelled as the hyperbolic nonlinearity which is a close practical approximation. The eigen value analysis at equilibrium points characterized the Hopf bifurcation of the system from stable to LCO mode. In the hopf bifurcation shown in figure 1.4, it is clearly seen that, up to certain value, there is only one stable equilibrium. After certain velocity, system develops two different stable equilibrium points. The state reached is based on initial condition of the system and even after this range of velocities system eventually settles to stable LCO. Beyond that range, unstable response occur. The analysis indicated the flutter onset velocity dependence on angular width $\pm \delta$ of free-play region. Figure 1.3 shows the flutter onset velocity dependence on free-play. It is clear that free-play nonlinearity lowers the flutter onset velocity and typically introduces a LCO mode of flutter. Results in the analysis indicate that an airfoil system susceptible to flutter shows pitchfork bifurcation at low airspeeds and hopf bifurcation at a moderate airspeed. This analysis using a simple 2D airfoil is very useful in understanding the free-play and flutter dynamics.

But analysing a complete three dimensional system is very complicated. It is very difficult to consider all kinds of dynamics into theoretical modelling. Hence wind tunnel models are built to simulate actual flow conditions and structural models to study more realistic and practical system dynamics. The Wright Air Development Centre (WADC) reports provide a good understanding of the experimental results. In order to develop the 3D system and wind

---

* Courtesy: VSI Aero, Ames, IA
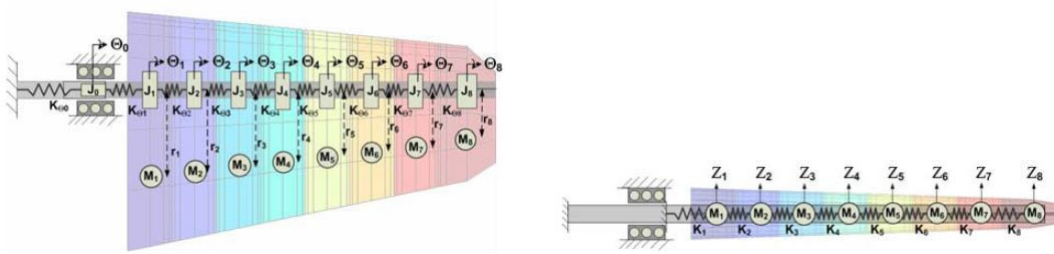
Figure 1.5   Schematic of WADC model [*]

tunnel experiments to study free-play and flutter interdependence extending the theoretical 2D understanding, different strategies to model 3D system are developed and also validated with the wind tunnel data and Air force results in WADC report. The work explained in Whitmer et al. (2012) closely modelled the WADC model as shown in figure 1.5. This work enabled more accurate high fidelity modelling of free-play and predicted the impact on flutter speed and frequency through various simulations.

The WADC 54-53 report has the test data for several different mounting locations of rotational axis out of which 33% of chord length is selected in the analysis. The models developed in the previous work used a low order panel code developed by researchers at Ames Research Center for modelling complex 3D bodies in potential flow. In Whitmer et al. (2012), different structural models are used with improved aeroelastic couplings and free-play is modelled as a nonlinear spring. The results obtained in simulations were validated using WADC report and successfully demonstrated methodology for modelling the interaction of aeroelastic dynamics and free-play for all moving surfaces. The test data in the WADC report was collected for numerous cases consisting of combinations of multiple values of free-play and root torsional spring stiffness. The theoretical model and the wind tunnel testing data showed that different values of free-play changes the LCO onset velocity and under specific free-play setting, LCO is sustained and bounded for a certain range of inflow velocities. If the flow velocity is increased beyond that range, divergence occurs. The work in this thesis is primarily based on exploiting the bifurcation characteristics of free-play dynamics in aeroelastic system response. In addi-

[*] Courtesy: VSI Aero, Ames, IA

tional to the theoretical and experimental approach followed in the study of aeroelastic response and its nonlinear dynamics, recent trend is to develop computational models of structure and fluid flow to incorporate different real world situations and transonic speed ranges as referred in Bennett and Edwards (1998), Silva and Bartels (2004). Computational Fluid Dynamics methods have been extensively developed and applied in the field of aeroelasticity. Many CFD codes coupled with structural dynamics and reduced order mathematical modelling techniques are used to study various aspects of flutter speeds, buffeting, LCO, buzz, Shock boundaries etc.as studied in Kim et al. (2005), Gupta (1996) Extensive computational power sometimes limit the computational analysis approach but most of the times it is proved advantageous over development of experimental set up, elapsed time, cost of labour and expensive peripheral processing.

As mentioned above, most of the approaches followed in the study of aeroelastic dynamics is focussed on the understanding of the phenomenon and development of control strategy to avoid this undesirable system response. Analytical, experimental computational approaches are used to analyse this dynamics response. It is also known that there is an energy exchange between fluid and structure that governs this interaction. There is increasing need to understand the energy transfer phenomenon taking place across fluid-structure interface. This area has not been explored sufficiently and motivates this research.

1.2   Motivation

Because of the highly destructive nature, flutter phenomenon has been topic of interest for researchers for a long time and yet, new discoveries emerge in understanding of flutter. One important aspect of flutter dynamics that has not been properly understood is the dynamics of energy transfer across the interfacing boundary. Recent literature in this field is focussed on the investigation of energy transfer pathways that form the basis of the aeroelastic flutter. In Patil (2002), Patil (2003) energy transfer between structure and fluid at various conditions is explained in case of flutter and flapping wings. The energy perspective used to develop different strategies to control flutter. It moves the system out of the unstable region of phase space by altering the critical flutter mode.

The other perspective looking at the flutter phenomenon is to understand the details of energy transfer that aids better design approaches as well as opens up the potential energy harvesting concept. Many different devices and strategies are develop to harvest energy from mechanical vibrations. Park et al. (2012), Bryant and Garcia (2011), Sousa et al. (2011), Erturk et al. (2010) gave a brief idea of harvesting mechanical vibrations. Generally smart materials like piezoelectric materials are used to convert vibrations into induced voltage.

A similar idea can be applied to this self feeding flutter vibrations in the aeroelastic response. When the fluid flow is pumping energy into the structure that sets the interaction into flutter mode, it can be extracted using a mechanism such that the constant oscillatory motion can be maintained. This perspective highlights the approach that flutter may not be always detrimental. A good understanding of energy transfer pathways in the system under flutter can shed light into qualitative and quantitative calculations of energy available for extraction. There is sparse of literature available on this and this approach motivates the work in this thesis.

The previous work in understanding flutter and free-play dynamics showed that flutter is dependent on free-play and under correct set of parameters characterizes hopf bifurcation, setting the system in sustained LCO mode. Also, results show that bounded LCO exist for a range of inflow velocities under one free-play setting. Combining these foundation results, need of understanding energy perspective and its harnessing potential give rise to the systematic step-by step approach followed in this work to qualitatively and quantitatively understand energy dynamics in aeroelastic response.

1.3 Objective

This study is focused on the energy perspective of the flutter response, i.e. to understand the fundamentals of energy interaction between fluid and structure and explore if there is potential to extract energy from flow field through structure for useful purposes. Keeping above motivation in mind, the objectives of this research are listed below:

- Model aeroelastic system with free-play nonlinearity and determine the parameters of the system to achieve stable LCO response over wide range of flow speeds. Use 2D configuration for detail analytical modelling of dynamic response and then transition to 3D configuration.

- Study energy interaction taking place at fluid structure interface and understand the sustained energy transfer from fluid to structure and structure to fluid.

- Develop energy harvesting concept and devise a strategy to explore if any excess energy imparted to the structure from the flow field can be harnessed in a sustained and effective manner. Develop a proof-of-concept harnessing mechanism and compute the energy extraction to assess energy harvesting potential

1.4 Approach

As stated previously the key motivation of this work is to explore how unstable flutter dynamics especially LCO can be exploited for the benefits rather than controlling it to avoid failures. As a result, the study is focussed on the energy recovery from aeroelastic response of the structure. The work in this thesis leverages the previous results given in Asjes (2015), Whitmer et al. (2012) and Asjes et al. (2014). The work demonstrating flutter dependence on free-play parameter, development of 2D system, modelling free-play as hyperbolic nonlinearity and wind tunnel experimental results presented before are used as the foundation for this thesis. This research extends this earlier work to gain deeper understanding of the aeroelastic response dynamics in the energy domain and highlights its energy extraction potential.

A representative 2D system similar to the one used in other literature (for example see-Asjes (2015)) is revisited and explained in details along with the free-play modelling using hyperbolic nonlinearity. Different candidate functions to model free-play are studied in details in Asjes (2015) and Asjes et al. (2014), but since hyperbolic function is the most suited practical approximation, it is used in this work. The plunge-pitch degree of freedom are imparted using torsional and linear springs. Once the dynamics of the system is simulated and the system is set in LCO mode, lift, aerodynamic moment, kinetic, potential and total energy variation are studied in details.

After gaining insights into energy transfer phenomena taking place in 2D configuration, high fidelity 3D computational model is developed. The wind tunnel experimental results from previous studies [Whitmer et al. (2012)] is used as a reference for the 3D computational model development to establish two way coupled system simulation. The energy evolution data obtained from 3D simulations was then studied in detail similar to the 2D case.

Once the qualitative and quantitative understanding of energy exchange is developed, its potential for energy extraction and harnessing is assessed. To devise an effective method to extract energy available in the system, mechanism using magnetostriction effect is proposed. Changing mechanical stresses developed in the structure due to dynamics system response are used to induce voltage in the coil. Magnetostrictive material-galfenol is selected to extract energy from the sustained oscillations over other smart materials because of its unique properties. This analysis is used to propose energy harvesting concept mechanism and controller design ideas for maximum throughput which gives a preliminary assessment of economic and technical viability of the concept.

The thesis is arranged as follows: A 2D system development is discussed in Chapter 2 followed by its energy analysis in Chapter 3. Details of previous wind tunnel model used as a basis for building computational model and the computational model itself are discussed in Chapter 4. Chapter 5 deals with the total two way coupled system set up and energy analysis for a 3D system. Concept of energy harvesting and corresponding mechanism along with the detail study of magnetostrictive material is documented in Chapter 6. Thesis contributions and future scope of the work is discussed in Chapter 7.

CHAPTER 2.   TWO DIMENSIONAL SYSTEM DEVELOPMENT

The aeroelastic response of the system is dependent on number of nonlinearities involved in fluid and structure. Theoretical analysis of fully coupled 3D aeroelastic system is complicated and, as a result, a simple 2D airfoil model is developed first and free-play non linearity is modelled such that a closed - form analytical model can be derived and the system can be studied in details from energy perspective. The airfoil system and free play non linearity parameters used are taken from Asjes (2015) to facilitate the validation of the model. This chapter deals with the complete derivation of equations used in 2D system analysis.

2.1   Description of the 2D model

A simple 2D airfoil with two degrees of freedom, namely plunge (h) and pitch (θ) is developed. Stiffness (K_h) and (K_θ) are attached for the plunge and pitch motion, respectively. Figure 2.1 shows the 2D airfoil system under consideration. Since the work presented in the thesis mainly deals with the energy approach, this 2D system definition is used as explained in Asjes (2015). Point ① is the aerodynamic centre assumed at the quarter cord length. This makes aerodynamic moment independent of angle of attack. All the aerodynamic forces- Lift and moment are assumed to act on the aerodynamic centre. Point ② is the elastic axis and system is assumed to rotate about this axis under pure rotational mode (pitching). i.e for 2D system, elastic axis is assumed to be coincident with the axis of rotation. Point ③ is the centre of gravity and all mass of the system is assumed to act through this point. E_{ac} is the eccentricity between aerodynamic centre and elastic axis, while e is the eccentricity between elastic axis and centre of gravity. These two eccentricities play important role in system dynamics as they decide the moments of the forces acting on the airfoil. This dislocation from the elastic
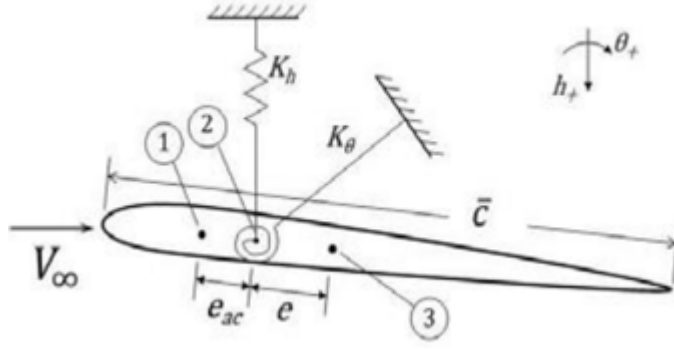
Figure 2.1   2D Airfoil System[*]

axis couples the pitching and plunging responses of the system. The values of the parameters used in the system are mentioned in Table 3.1.

The energy based approach is used in the derivation of equation of motion such that the external aerodynamic forces balance the structural forces. Following is the equation of the motion is set up taking into consideration inertia and stiffness of the system:

$$
M_s \begin{bmatrix} \ddot{h} \\ \ddot{\theta} \end{bmatrix} + K_s \begin{bmatrix} h \\ \theta \end{bmatrix} = F_{aero} \tag{2.1}
$$

where,

$$
M_s = \begin{bmatrix} m & -me \\ -me & me^2 + j \end{bmatrix} ; \qquad K_s = \begin{bmatrix} k_h & 0 \\ 0 & K_\theta \end{bmatrix} ; \qquad F_{aero} = \begin{bmatrix} -L_a \\ M_a \end{bmatrix} ; \tag{2.2}
$$

Lift and moment acting because of the external fluid flow over the airfoil acts as the external forcing functions and are assumed as the function of angle of attack (α), angle of attack rate $(\dot{\alpha})$,and pitch rate $(\dot{\theta})$. These forces and moments are expressed in terms of classical non-dimensional forces and moment coefficients which are valid for both steady and unsteady aerodynamics. Use of aerodynamic coefficients indicates that the model is linearization of

---

[*]Taken from Asjes(2015)

nonlinear aerodynamics. Following equations are used:

$$L_a = \bar{q}S(C_{L\alpha}\alpha + C_{L\dot{\alpha}}\dot{\alpha} + C_{Lq}q) \tag{2.3}$$

$$M_a = \bar{q}S\bar{c}(C_{M\alpha}\alpha + C_{M\dot{\alpha}}\dot{\alpha} + C_{Mq}q) + \bar{q}Se_{ac}(C_{L\alpha}\alpha + C_{L\dot{\alpha}}\dot{\alpha} + C_{Lq}q) \tag{2.4}$$

Where, $\bar{q}$ is dynamic pressure and $\bar{c}$ is chord length. Second term in the moment equation is transferring the lift to elastic axis due to eccentricity assumed in the model. For the complete aerodynamic model, dependent variables of the aerodynamic equations are converted to the state variables of structure using following substitution:

$$\alpha = \theta + \frac{\dot{h}}{V}; \qquad \dot{\alpha} = \dot{\theta} + \frac{\ddot{h}}{v}; \qquad q = \dot{\theta} \tag{2.5}$$

Substituting this back in Lift and moment equations:

$$L_a = \bar{q}S\left[C_{L\alpha}\left(\theta + \frac{\dot{h}}{V}\right) + C_{L\dot{\alpha}}\left(\dot{\theta} + \frac{\ddot{h}}{V}\right) + C_{Lq}\dot{\theta}\right] \tag{2.6}$$

$$M_a = \bar{q}S\bar{c}\left[C_{M\alpha}(\theta + \frac{\dot{h}}{V}) + C_{M\dot{\alpha}}(\dot{\theta} + \frac{\ddot{h}}{V}) + C_{Mq}\dot{\theta}\right] + \bar{q}Se_{ac}\left[C_{L\alpha}\left(\theta + \frac{\dot{h}}{V}\right) + C_{L\dot{\alpha}}\left(\dot{\theta} + \frac{\ddot{h}}{V}\right) + C_{Lq}\dot{\theta}\right] \tag{2.7}$$

Decomposing the external forcing function contributions in terms of mass, stiffness and damping of coupled system:

$$F_{aero} = M_{app}\begin{bmatrix}\ddot{h}\\\ddot{\theta}\end{bmatrix} + B_a\begin{bmatrix}\dot{h}\\\dot{\theta}\end{bmatrix} + K_a\begin{bmatrix}h\\\theta\end{bmatrix} \tag{2.8}$$

Where,

$$M_{app} = \bar{q}S\begin{bmatrix}\frac{-C_{L\dot{\alpha}}}{V} & 0\\\frac{\bar{c}C_{M\dot{\alpha}}+e_{ac}C_{L\dot{\alpha}}}{V} & 0\end{bmatrix}; K_a = \bar{q}S\begin{bmatrix}0 & C_{L\alpha}\\0 & \bar{c}C_{M\alpha} + e_{ac}C_{L\alpha}\end{bmatrix}; \tag{2.9}$$

$$B_a = \bar{q}S\begin{bmatrix}\frac{-C_{L\alpha}}{V} & -(C_{L\dot{\alpha}} + C_{Lq})\\\frac{\bar{c}C_{M\alpha}+e_{ac}C_{L\alpha}}{V} & \bar{c}(C_{M\dot{\alpha}} + C_{Mq}) + e_{ac}(C_{L\dot{\alpha}} + C_{Lq})\end{bmatrix} \tag{2.10}$$

Combining this with Eq (2.1) we get,

$$(M_s - M_{app})\begin{bmatrix}\ddot{h}\\\ddot{\theta}\end{bmatrix} = B_a\begin{bmatrix}\dot{h}\\\dot{\theta}\end{bmatrix} + (K_a - K_s)\begin{bmatrix}h\\\theta\end{bmatrix} \tag{2.11}$$

$$
\begin{bmatrix} \ddot{h} \\ \ddot{\theta} \end{bmatrix} = (M_s - M_{app})^{-1} B_a \begin{bmatrix} \dot{h} \\ \dot{\theta} \end{bmatrix} + (M_s - M_{app})^{-1} (K_a - K_s) \begin{bmatrix} h \\ \theta \end{bmatrix} = D \begin{bmatrix} \dot{h} \\ \dot{\theta} \end{bmatrix} + E \begin{bmatrix} h \\ \theta \end{bmatrix} \quad (2.12)
$$

Since the aeroelastic motion comprises of pitching and plunging modes, $\begin{bmatrix} h \\ \theta \end{bmatrix}$ the state vector for analysis is defined as:

$$
x = \begin{bmatrix} h & \theta & \dot{h} & \dot{\theta} \end{bmatrix}^{\top} \quad (2.13)
$$

The aeroelastic response is considered in this thesis, is due to the free-play non linearity induced in the rotational stiffness. Hence terms containing rotational stiffness i.e., (K_θ) are only non linear terms. Separating nonlinear terms with linear terms, we get

$$
\dot{x}_1 = x_3
$$

$$
\dot{x}_2 = x_4
$$

$$
\dot{x}_3 = E_{11} x_1 + (E_{12L} x_2 + E_{12NL} \hat{x}_2) + D_{11} x_3 + D_{12} x_4
$$

$$
\dot{x}_4 = E_{21} x_1 + (E_{22L} x_2 + E_{22NL} \hat{x}_2) + D_{21} x_3 + D_{22} x_4
$$

where

$$
E_{12NL} = \frac{-Vem}{|M_s - M_{app}|} K_\theta; \qquad E_{22NL} = \frac{-(Vm + C_{L\dot{\alpha}} \bar{q} S)}{|M_s - M_{app}|} K_\theta \quad (2.14)
$$

The state space for of the system is:

$$
\dot{x} = \begin{bmatrix} 0 & I \\ E_L & D \end{bmatrix} x + E_{NL} \hat{x}_2
$$

The nonlinear term $\hat{x}_2$ is now defined using a function $\phi(\theta)$, which is actually a modelling of free-play non linearity explained in next section. This way, rotational stiffness is modelled as nonlinear function and substituted in the state space dynamics of the system. Separating the terms and introducing free-play non linearity, the state space representation of the system is:

$$
\dot{x} = Ax + B\phi(\theta); \quad y = cx \quad (2.15)
$$

2.2 Modelling of free-play nonlinearity

In literature different type of nonlinear functions are used to model free-play nonlinearity but as showing Asjes (2015) hyperbolic nonlinearity is found to be the best suited from the perspective of analytical development. The details of candidate functions like cubic nonlinearity and piecewise linear function are studied in details in Asjes (2015) . Analysis shows that, a piecewise linear function is easy to implement as a free-play nonlinearity but does not provide much insights into flutter characteristics.

Second candidate function studied was cubic function which is often used to model torsional nonlinearity. The general formulation used for cubic nonlinearity is

$$\phi_{cub}(\theta) = \beta_1\theta + \beta_3\theta^3 \tag{2.16}$$

But this formulation does not fully captures the nonlinear LCO behaviour and Hopf bifurcation expected in the response and hence not selected for free-play modelling.

2.2.1 Hyperbolic Function

Hyperbolic function captures expected and observed nonlinear response. This nonlinearity is the best practical approximation of the free-play observed in rotational joints. Figure 2.2 shows the representation of hyperbolic nonlinearity.

The Hyperbolic functionused to model the free-play nonlinearity is given by

$$\phi(y) = sgn(y)\left(\frac{\gamma_1 + \gamma_2}{2}(|y| - \delta) + \left[\frac{(\gamma_2 - \gamma_1)^2 + (|y| - \delta)^2 + 4\gamma_1\gamma_2\delta^2}{4}\right]^{\frac{1}{2}}\right) \tag{2.17}$$

where

- γ_1 and γ_2 are asymptotic slopes and vertex of the hyperbola is chosen at the edge of the free-play region.

- Hyperbola must pass through origin i.e. $\phi_h(0) = 0$;

- Asymptotic slope in free-play region is γ_1

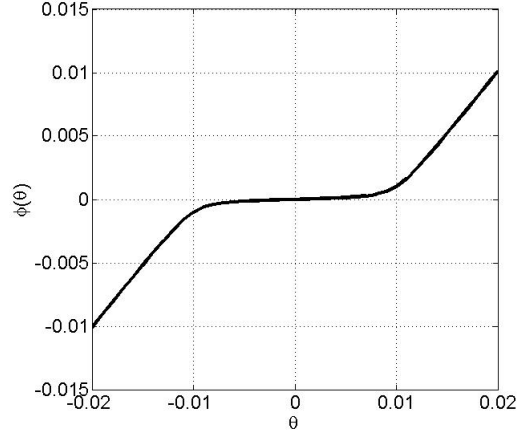- The asymptotic slope of hyperbola as $\theta \to \infty$ is γ_2. This sets the slope in linear region.

Figure 2.2   Hyperbolic Nonlinearity

Following are the conditions imposed on the function

1. The limiting stiffness as $y \to \infty$ is linear stiffness of the spring, $\gamma_2 = 1$.

2. As free-play increases ($\delta \to \infty$), nonlinear stiffness converges to a piecewise linear stiffness. $\lim_{\delta \to \infty} \gamma_1 = 0$.

3. As free-play decreases ($\delta \to 0$), nonlinear stiffness converges to linear stiffness $\Rightarrow \lim_{\delta \to 0} \gamma_1 = \gamma_2 = 1$.

Using these conditions, $\gamma_1 = \frac{1}{1+\alpha_\gamma \delta^r}$ is used. Values of the nonlinear parameters are chosen to adjust as per model.

With this nonlinearity model a complete set of 2D aeroelastic system with free-play in rotational degree of freedom are given as:

$$\dot{x} = Ax + B\phi(\theta); \quad y = cx$$

CHAPTER 3. TWO DIMENSIONAL SYSTEM ANALYSIS

In the previous chapter, a complete theoretical foundation for 2D aeroelastic system along with free-play nonlinearity was discussed. This chapter deals with the simulation of the aeroelastic system response and analysis of the response. The simulation is performed in the Matlab environment. The main objective of this analysis is to understand dynamic response of the structural system during different phases and associate energy exchange that take place between structure and surrounding flow field. The response of the system is analysed by looking at the time evolution of various states of the system and computing both kinetic and potential energies of the system during this evolution of the response. The parametric studies are also performed to see the effect of varying parameters of the system and also the flow speeds on the aeroelastic response and energy exchange.

3.1 2D System simulations

The state space representation of the system along with hyperbolic free-play nonlinearity is modelled in Matlab using the parameter values mentioned in the Table 3.1. Lift and aerodynamic moment are calculated using equations (2.6), (2.7). Also, the state vector x is calculated for simulation time with constant time step.

Table 3.1   System parameters and initial condition

Parameter	Value	Parameter	Value
Mass, m	$4.04 slugs$	$C_{L\alpha}$	3.5860
Moment of inertia, J	$16 slug.ft$	$C_{L\dot{\alpha}}$	0.0230
Chord length, $\bar{c}$	$10in$	C_{Lq}	0.0386
Bending stiffness, K_h	$2,500 lb_f/in$	$C_{M\alpha}$	2.934
Torsional Stiffness, k_θ	$21,000 ftlb_f/rad$	$C_{M\dot{\alpha}}$	-0.0103
Eccentricity, e_{ac}	$-0.15in$	C_{Mq}	-0.025
Delta, δ	0.01	γ_2	1
r	100	α_γ	100
Initial Condition $(h, \theta, \dot{h}, \dot{\theta})$	$0.1, 0.05, 0.02, 0.01$	Flow Velocity	$13.3 fps$

3.2   System response under LCO

First, lift vs plunge velocity $(\dot{h})$ and aerodynamic moment vs pitch velocity $(\dot{\theta})$ are plotted in one cycle to study the limit cycle established in the system. For the given simulations system is assumed to start with non zero initial condition given as $[0.1\ 0.05\ 0.02\ 0.01]^\top$.

Since the purpose of this study is to understand the system response in sustained LCO, inflow velocity, other system parameters and nonlinearity parameters are adjusted such that after non zero initial condition, system settles down to sustained LCO. This can be seen from figures 3.1 and 3.2. These figures show that after first few iterations, system eventually settles down to sustained oscillations with approximately same magnitude.
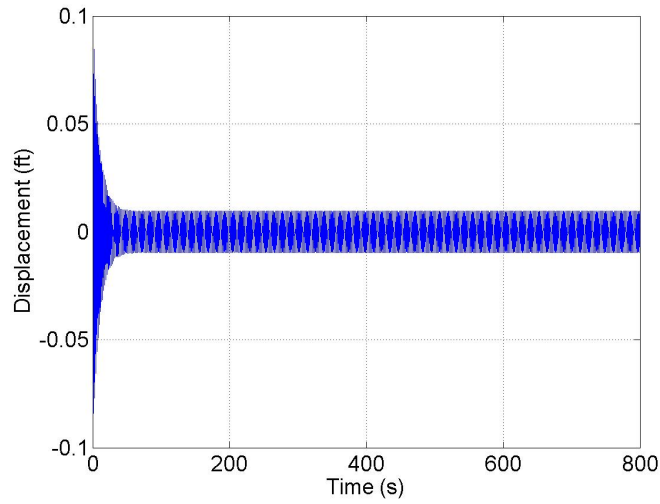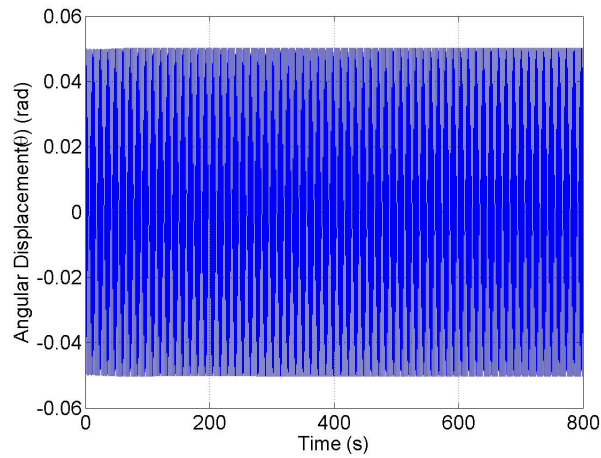
Figure 3.1   Displacement vs Time

Figure 3.2   Angular Displacement vs Time

The previous study showed that the LCO state exists for a range of inflow velocities. Once the LCO sets in, further plots are studied to understand the details of aeroelastic response. Lift and aerodynamic moments are calculated for given interval of time which also shows the stable LCO response once the system equilibrium is set to LCO. Figures 3.3 and 3.4 show the lift and moment response for given simulation time.
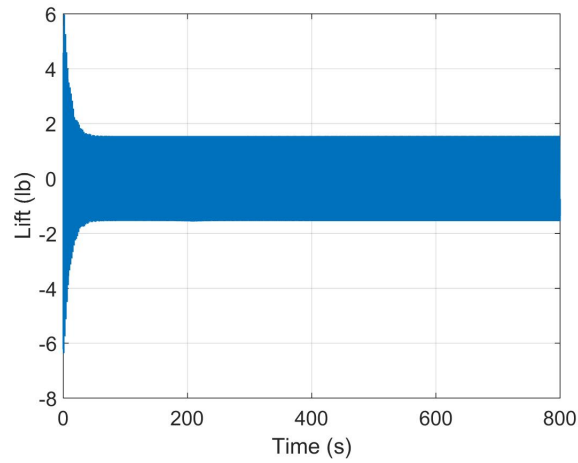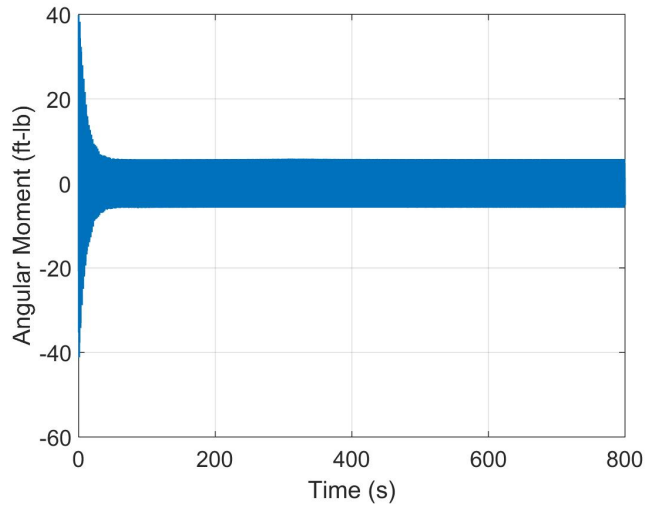
Figure 3.3   Lift vs Complete time

Figure 3.4   Aerodynamic Moment vs Time

These figures give the overall picture of system response during the complete simulation time. More insights on what happens in individual cycle is obtained by plotting the system response in only last cycle.
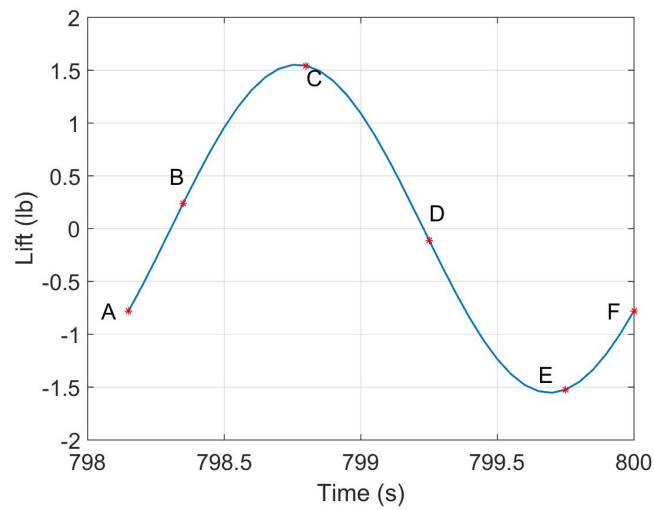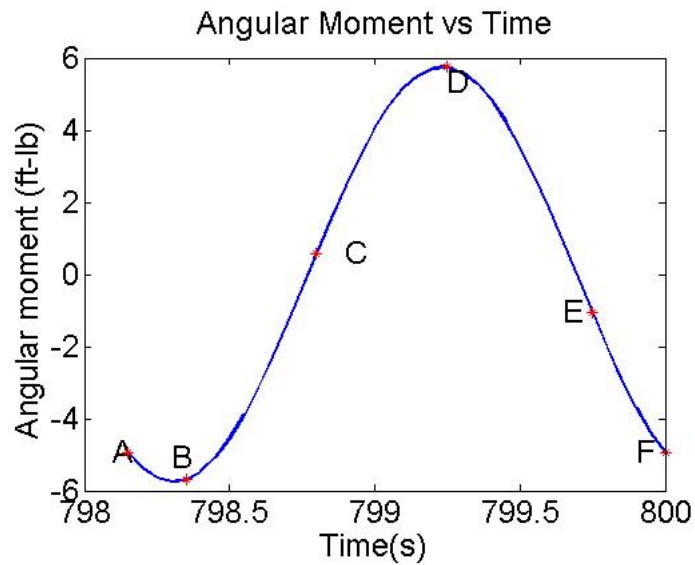
Figure 3.5   Lift vs Time in one cycle

Figure 3.6   Aerodynamic Moment vs Time in one cycle

Figures 3.5 and 3.6 show how lift and aerodynamic moment changes in one cycle. Points A,B,C,D,E,F are helpful in tracing the changes in varying quantities. Later, these points are related to energy variation in one cycle.
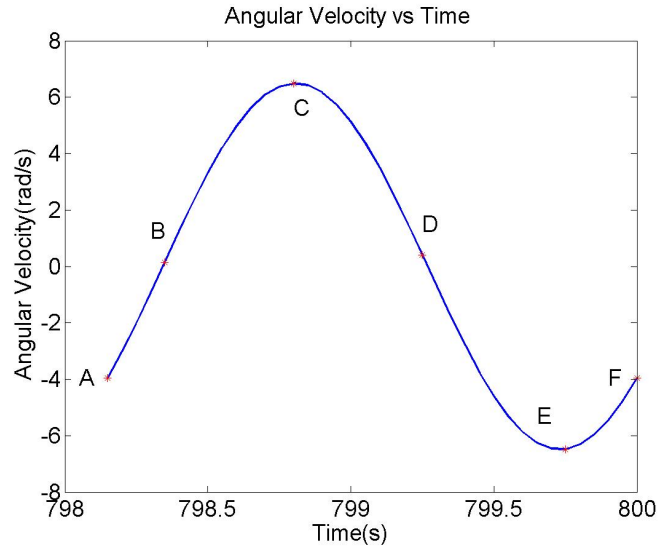
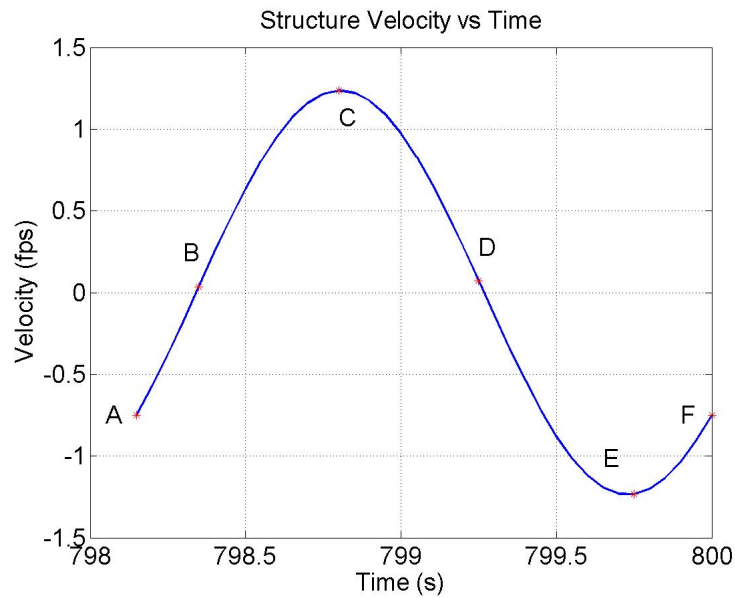Figure 3.7   Pitch Rate vs Time

Figure 3.8   Plunge Rate vs Time

Figure 3.7 shows how pitch rate is developed in one cycle and figure 3.8 shows the variation in plunge rate. The points marked on these plots along with lift and moment variation in one cycle are used to understand closed plots of Lift vs Plunge velocity and Moment vs Pitch

velocity in one cycle.

Figures 3.10 and 3.9 show closed cyclic nature of lift and moment variation with respect to plunge and pitch rate respectively. This shows the LCO response. Lift and moment are the external aerodynamic forces acting on the airfoil. Plunge and pitch are the two modes depicted by the structure. During the motion of aeroelastic structure, the change in the structural states results in an instantaneous change in the flow field. This alters the pressure fields eventually changing the flow energy. The rate of this energy exchange is also called the energy flux at the aero-structure boundary.

Figure 3.9   Moment vs Pitch Rate
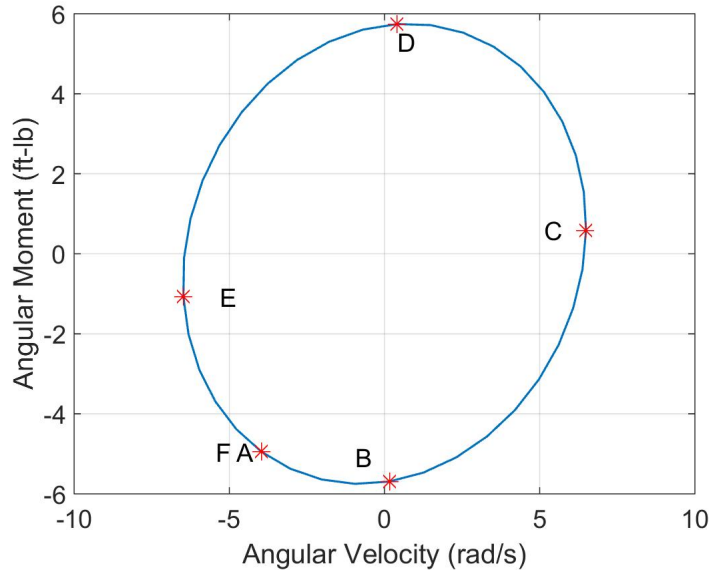
The energy flux across the aero-structure boundary cycles periodically over time, and is usually dissipative in nature, describing elliptical trajectories in the lift- plunge rate (moment-pitch rate) plane. The energy flux that is generated at the airfoil/flow field interface is determined by calculating the rate at which lift and moment do work on the airfoil system at each time-step.
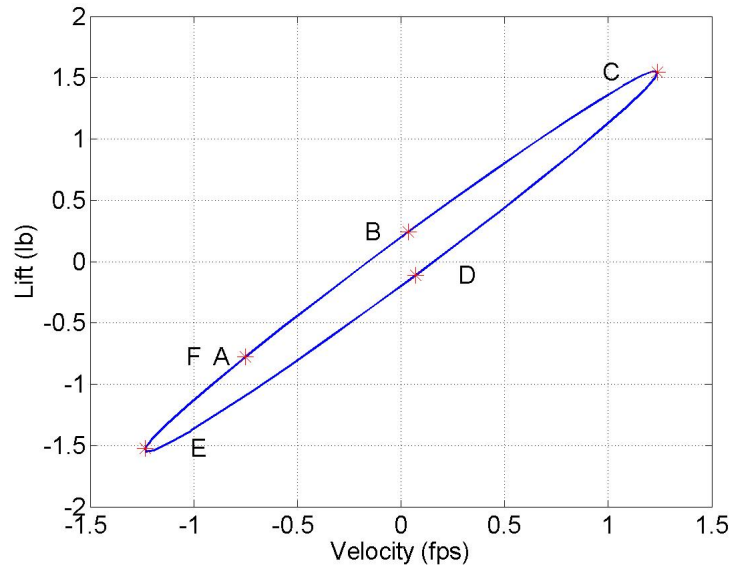
Figure 3.10   Lift vs Plunge Rate

Figure 3.9 depicts a time plot of airfoil aerodynamic moment vs pitch rate. The curve represents a single cycle of oscillatory motion. The net flux from flow field to structure being positive or negative, dictates whether the system is in a flutter state or a non-flutter state, respectively. If the net flux from the flow field to the structure is negative then the structure dissipates energy and is stable. Figure 3.10 shows a similar situation for energy flow in the plunging motion of the airfoil.

3.3   Energy analysis of 2D system

In order to better understand the energy exchange phenomena, the time evolution of kinetic, potential and total energy are plotted for one representative cycle of the response. Points A,B,C,D,E,F are plotted on the graph to trace the different stages in the energy transfer. Figures 3.11 and 3.12 show potential and kinetic energy in one cycle. The cyclic variation of energy is evident from the plot. It is clearly seen that, when kinetic energy increases potential energy decreases and vice a versa.
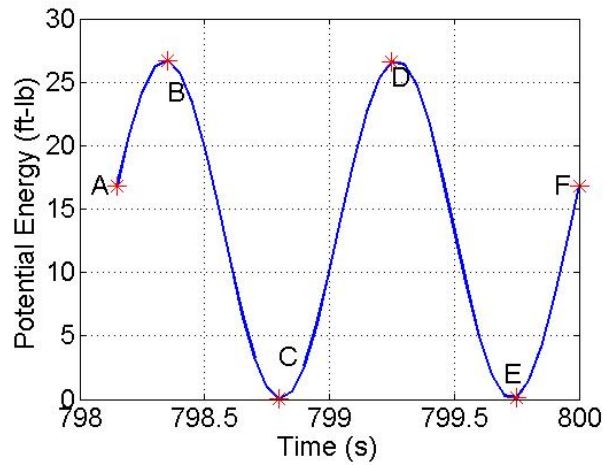
Figure 3.11   Potential Energy vs Time in one cycle

The acceleration and total energy variation in one cycle plots are studied in detail, to trace how energy is varying in one cycle. The points B,C,D,E marked on figure 3.14 represent points where direction of energy flow is reversed between structural system and flow field.
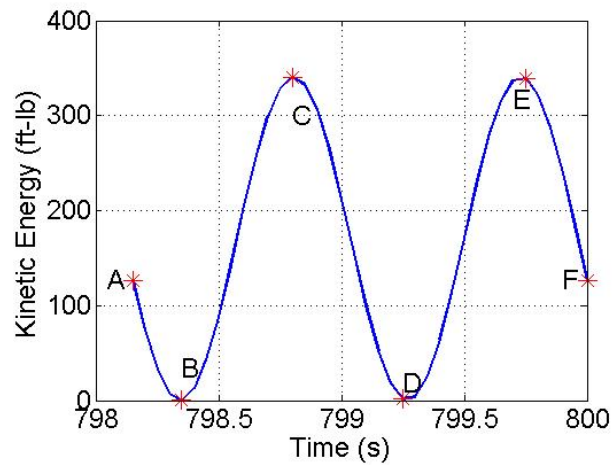

Figure 3.12   Kinetic Energy vs Time in one cycle

Segment AB, CD, EF indicate parts of the cycle where energy is transferred from structure to the flow field whereas the plot segments BC and DE indicate the parts of the cycle where energy is transferred from flow field to the structure under the correct set of parameters. This

energy exchange is balanced and as a result a stable and bounded LCO is obtained. This understanding can further be explained from acceleration rate of structure in given representative cycle. It is seen that, increase in acceleration means structure is transferring energy to fluid lowering the total energy and decrease in acceleration means fluid is giving energy to structure increasing the total energy of the structure. If the energy flow into the flow field exceeds the flow into the structure the total energy of the structural will dissipate over time due to aerodynamic and structural damping and structure will come to rest.
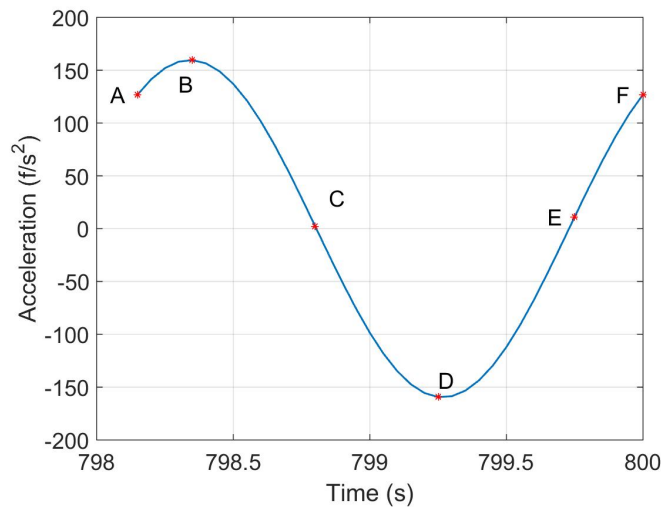
Figure 3.13   Acceleration vs Time in one cycle
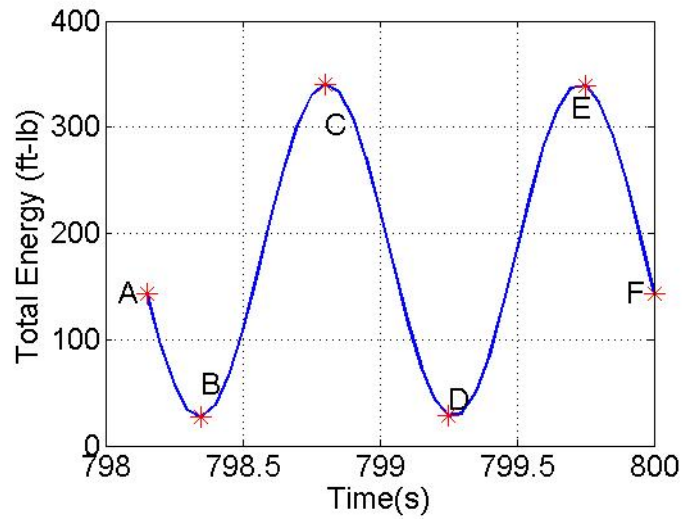
Figure 3.14   Total Energy vs Time in one cycle

On the other hand if the energy flow into the structure exceeds the energy flow back into the flow field the total energy in the structural will keep increasing leading to divergent response of the structure which will eventually cause failure of the structure. In the case of stable bounded LCO, all this energy transfer across fluid-structure interface is balanced and this can be seen from the total energy plot for complete simulation time.

Figure 3.15   Total Energy vs Time

The figure 3.15 shows that system starts with some nonzero energy value (39 ft-lb) and eventually as iterations proceed stabilizes into LCO i.e., balanced energy transfer. This detailed understanding of energy and balanced energy transfer in LCO opens up the potential of energy harvesting. The LCO on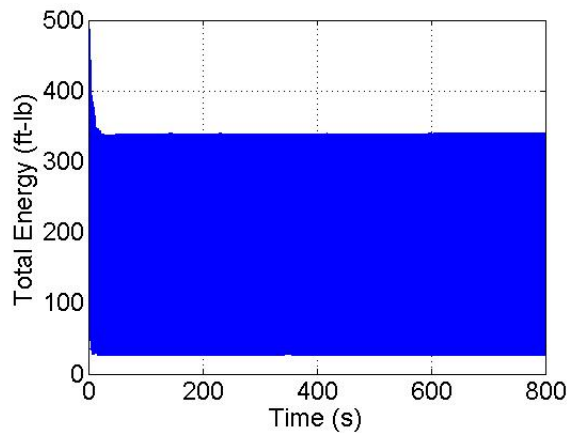set velocity depends on several factors but in a simple 2D case shown here, it mainly depends on inflow velocity and free-play parameters. If we can adjust these parameters to suit the changing inflow conditions and maintain the LCO for sustaining energy output, a good energy harvesting concept can be developed. The harvesting ideas and available energy quantification is studied in detail in Chapter 6.

In summary, this chapter presented qualitative and quantitative understanding of energy transfer involved in the aeroelastic response of the system. Based on the results of 2D analysis from this chapter, a higher fidelity 3D model is developed and energy dynamics involved in that system is studied in the next chapter.

CHAPTER 4. THREE DIMENSIONAL MODEL DEVELOPMENT

In the previous chapters, a complete development of 2D aeroelastic system and dynamics of energy exchange were studied in detail. Modelling 2D system can be done in closed form using analytical techniques, but 3D modelling with coupled system analysis is complex and often requires computational methods and validation through wind tunnel experiments. In this work, a higher fidelity computational model of fully coupled fluid-structure interaction is developed using Ansys. The model is then simulated for different flow conditions and initial excitations.

This computational model is developed using the parameters of the experimental model tested in wind tunnel as shown in figure 4.1. The experiments are not a part of this thesis work, but are used here as a reference to develop high fidelity computational model. This also enables the validation of the data obtained from the computational model. Details of the experimental model developed earlier is discussed in the later part of the chapter. The model is built similar to the one developed by US Air force in mid-1950s [Hoffman and Spielberg (1954)]. This chapter deals with detailing of the experimental model development and computational model motivated from that. Commercial code-Ansys is used to develop computational model and it is coupled to fluid domain using the special system coupling module.

4.1 Revisiting experimental model development

For the experimental purpose, eight section model was constructed and used in wing tunnel. The main motivation for this modelling strategy is to allow close matching of modal parameters and other results as published in WADC report- Hoffman and Spielberg (1954). Hence the experimental model is the replica of the WADC model shown in figure 1.5.The modal charac-

teristics, moment of inertial and segment masses etc. are matched such that the replica closely tied with the WADC modal enabling use of its results for validation. Figures 4.1 and 4.2 show the experimental model developed and mounted in wind tunnel.

The model comprises of 8 sections using NACA 0012 airfoil. The aerodynamic centre (x_{ac}) is assumed at quarter cord point and an elastic axis is assumed at 33% of the chord.

Figure 4.1   Experimental Setup (front)*
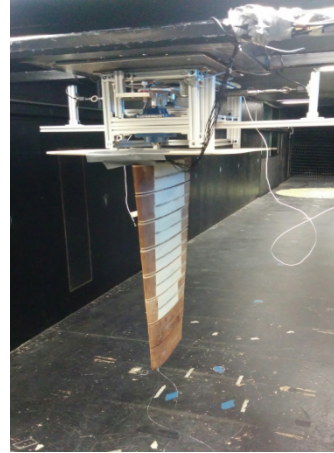
Figure 4.2   Experimental Setup (side) *
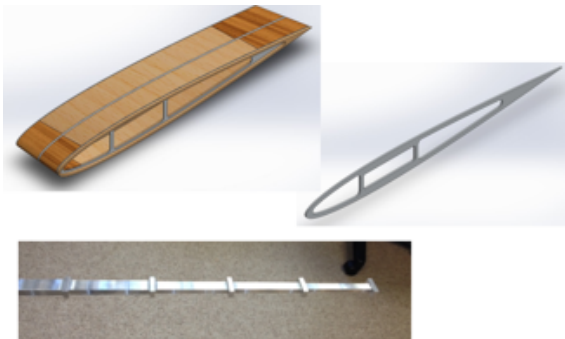
Figure 4.3   Individual Section *

Figure 4.4   Internal Structure *

Each section is designed to be 4 inch in span. The segments are arranged such that the elastic axis runs perpendicular to the inflow velocity direction. Each segment has a slightly smaller chord length giving taper to the model. Axis of rotation is assumed to be along the elastic axis. This assumes no stiffness coupling between pitch and plunge modes. But its influence is seen

---

* Courtesy: VSI Aero, Ames, IA

in the dynamics of each segment. All these 8 sections are attached independently to the single aluminium spar, rectangular in cross-section and tapered along its length in stair-step fashion as shown in figure 4.3. Each section is built around an aluminium centre rib which is only connected to the central spar. This makes effective concentration of forces and moments at the descrete location throughout the spar. To maintain the elastic axis as axis of rotation, each middle segment is connected to the spar at the elastic axis location as shown in figure 4.4.Other airfoil sections one on each side is separate from the spar but shares the balsa skin covering the entire section. Mahogany wood skin is attached near leading and trailing edges. The moment of inertial of the single section is maintained such that the overall moment of inertial matches with the WADC model. The model was mounted vertically in the wind tunnel using free-play control mechanism. The free-play mechanism is connected to the free spar end implementing the rotational free-play boundary condition. The mechanism and connection is as shown in the figure 4.5. By adjusting the top plat and pin, various magnitudes of the free-play can be implemented. This arrangement was used in the experiment to study the flutter onset velocity dependence on free-play.
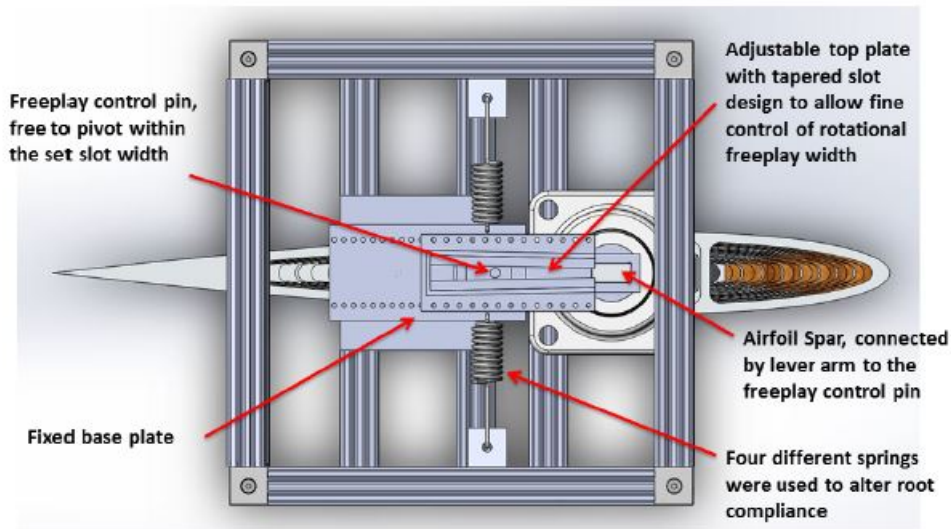

Figure 4.5   Free-play Mechanism *

* Taken from Asjes (2015)

This model is tested in Wind Simulation and Testing Laboratory (WiST Lab) in the Department of Aerospace Engineering at Iowa State University. The airfoil was instrumented with potentiometer at the root to measure angular rotations and pair of accelerometers at each section. The non-zero initial condition to start the dynamic response is given by manual impulse excitation.

4.2 Computational model development

The computational model developed in this section is closely tied to the experimental model explained above. The geometry and modal characteristics are maintained to suit the experimental set up. Geometry is built up in Ansys APDL - Ansys (b). Figures 4.6 and 4.7 show the computational model and important dimensions involved.
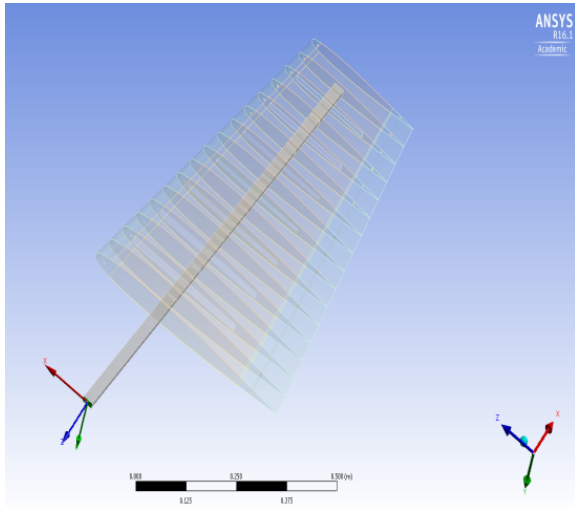
Figure 4.6   Computational Model
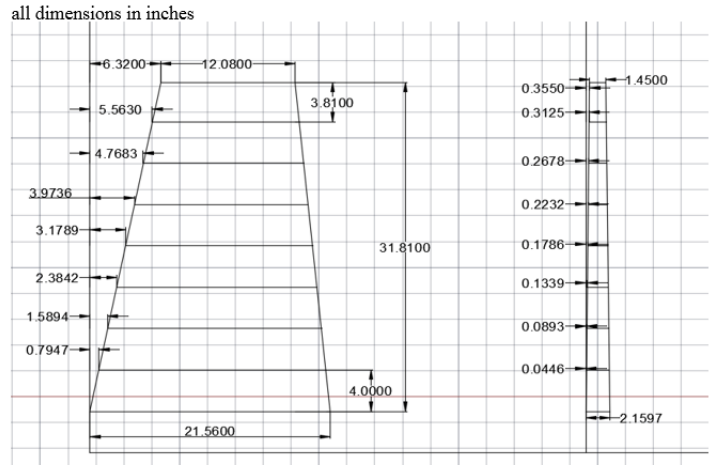
Figure 4.7   3D Model Dimesions

Similar to experimental model, this computational model consists of 8 sections and a spar running in the elastic axis location (33% of chord length). The central ribs in each section is connected to the spar at corresponding intersection using node coupling. Other two supporting ribs connect to the entire section through covering skin. A covering skin defined as shell element is attached to the entire sections connecting side supporting ribs. The slots in the

airfoil sections are made representative of the model balancing the modal characteristics. Spar in the computational model is assumed to be same cross-section and made through volume extrusion using solid elements. Two small bars with circular cross-section are designed passing through all sections for the strength and stiffness to the model. All the specific material types and properties used in the model are as shown in Table 4.1.

Table 4.1   List of Material Properties

Geometry	Material	Density ($\frac{kg}{m^3}$)	Young's Modulus ($\frac{N}{m^2}$)	Poisson's Ratio	Thickness(m)
Spar	Aluminium	2810	71.7e9	0.33	
Ribs	Aluminium	2810	71.7e9	0.33	0.003
Skin Middle Part	Balsa	130	3e9	0.3	0.015
Skin Towards Edges	Mahogany	420	7.9e9	0.29	0.015

All parts in the model are meshed with suitable sizes and corresponding material type and properties. This model is simulated for zero-free play condition and hence the free spar end which is connected to the free-play mechanism in the wind tunnel is subjected to fixed boundary condition. (all DOF = 0)

4.3   Modal analysis of computational model

Modal analysis is performed for the above developed model. The dominant mode of interest is bending and torsion. This is extension of pitching-plunging action analysed in 2D case. Hence out of different modes for this boundary condition and arrangements, bending-torsion mode is considered for further analysis and when the fluid-structure interaction is set up in system coupling, inflow velocity is set such that this mode of interest is excited. Figure 4.8, figure 4.9 and figure 4.10 show the first three modes of the flexible structure. Firth two modes being the in plane and out of plane bending, third mode is the bending - torsion mode. Once the modal characteristics of the model are obtained confirming all the components are properly connected and mass properties and distribution are within accepted approximation, the model is further taken to the coupled system analysis.
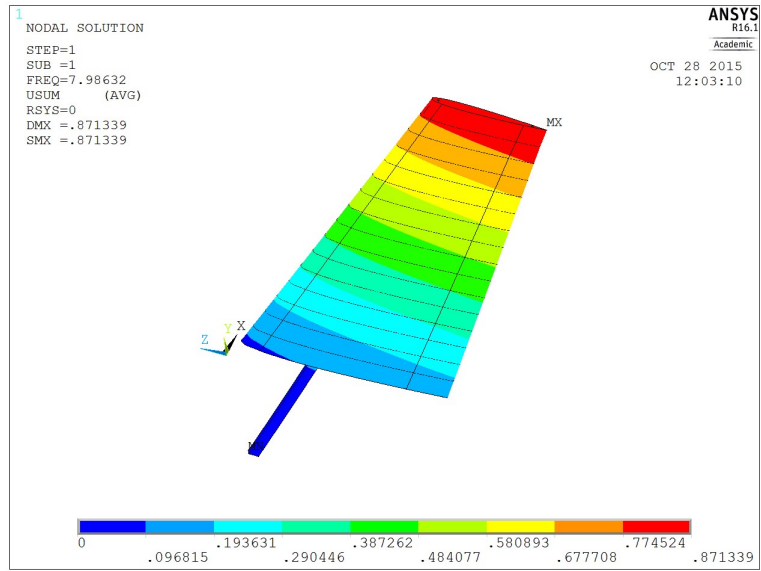
Figure 4.8   Mode 1
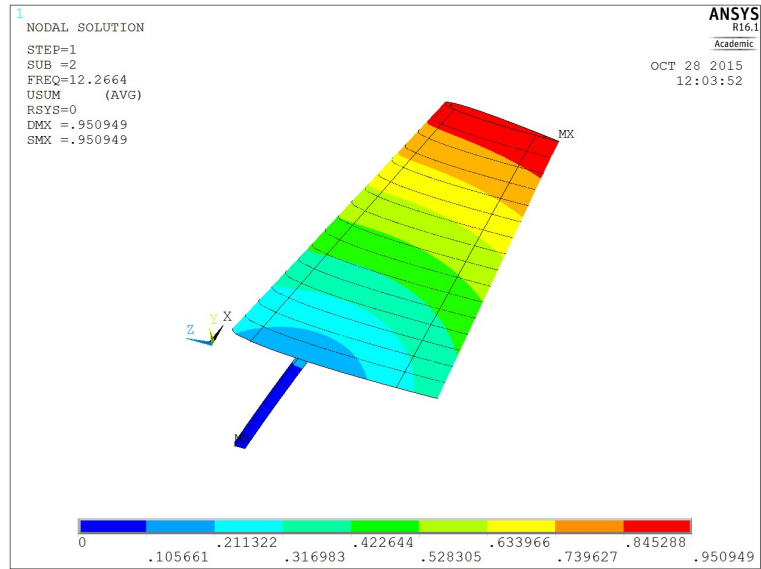
Figure 4.9   Mode 2

Figure 4.10   Mode 3

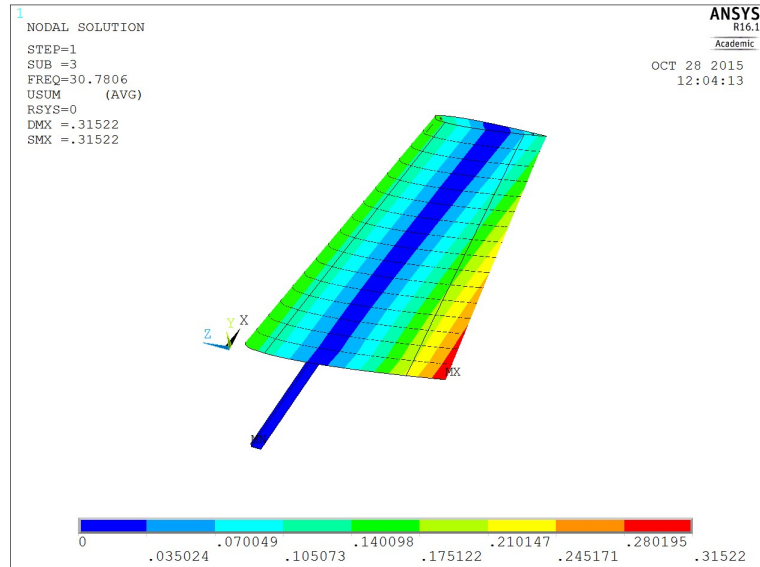The modal characteristics are further adjusted by adding point mass at specific location exactly matching the mass of inertia properties of the each section in the experimental set up. But this modification is not discussed here. Setting up the coupled simulation using complete model is computationally very expensive and time consuming. Hence only one section of model is considered for further analysis.

CHAPTER 5.   THREE DIMENSIONAL SYSTEM ANALYSIS

The previous chapter presented, the details of 3D model development. This chapter extends the energy domain analysis conducted for a 2D configuration in Chapter 3 to 3D system and gaons insights into the energy interaction in 3D aero-structure model. The chapter begins with explanation of the simulation set up and then presents energy analysis and associated observations.

5.1   Two way system coupling using Ansys Workbench

In the aeroelastic dynamics there is fluid structure interaction at the interface where flexible structure displaces fluid changing its pressure field. This changed pressure field changes the aerodynamic forces acting on the structure changing structural deformations. So there is a cyclic exchange between forces and structural deformation. This takes place due to aeroelastic coupling between structure inertia, elasticity and aerodynamics. This is a nonlinear dynamics and it can be stable or unstable based on system parameters and operating conditions. In order to model this interaction in Ansys, two way data transfer is set up using Ansys (f). The output of structure subsystem, displacement, is input to the fluid solver that calculates the new aerodynamic forces acting on the structure. These forces acts on the structure causing structural motion which in turn displaces fluid around it and the cycle continues. Figure 5.1 shows this cyclic two way data transfer.
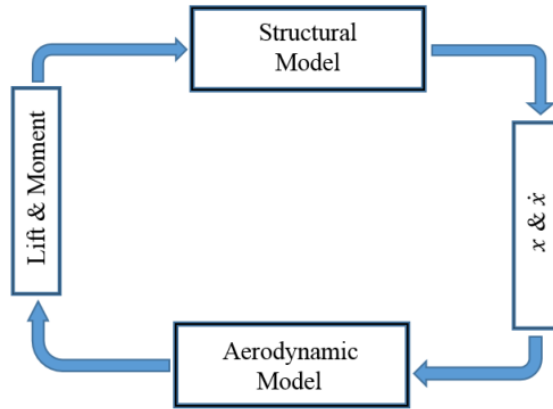
Figure 5.1   Two Way Data Transfer

The coupling of transient fluid-structure systems in Ansys uses co-simulation technique to analyze the interaction. The source- target relationship is maintained and two way (from transient structural to transient fluid and vice a versa) data transfer is established. In the model under consideration, fluid-structure interface is defined in the structural module and it is coupled with the corresponding surfaces in the fluid domain using dynamic meshing. The structural displacement and force exerted by fluid flow are transferred at this interface [Ansys (e), Ansys (f)].

The analysis is based on coupling steps and number of iterations in each step. Root Mean Square (RMS) convergence is used and when two successive iterations produce a normalized value under convergence target, the data transfer is assumed to have converged. Duration of coupled analysis is broken into sequence of coupling steps. Data transfer between solvers occurs at the beginning of each coupling iteration within coupling step. New coupling step is started either when maximum number of coupling iterations has been reached and coupling analysis duration has not been reached or coupling step is converged. In the analysis settings, minimum and maximum number of coupling iterations within coupling step can be specified. Also, step size is specified which is defined in terms of time interval. It specifies the time interval (in sec) associated with each coupling step. For the system under consideration, step time is decided to be 0.001 s. There are many factors affecting the choice of time step. It depends on the type

of analysis, meshing size, accuracy of result etc. In the system under consideration, meshing size and coupling time step is decided such that the transient dynamic analysis is performed without creating any negative volumes during data transfer. Since transient structural module is used, coupling step size is same as transient structural step size. The simulation is run for multiple coupling steps using end of coupling step as a restart point if needed. This enables more restart points if the run is terminated unexpectedly.

5.2   Steps in setting up Workbench interface

Above section gives some physical understanding of the process involved in two way data transfer. This section deals with the detail steps involved in setting up the interface. The system geometry is created as explained in Chapter 4. But coupled simulation with very high number of nodes and fine meshing was computationally very expensive and time consuming. Hence a smaller model consisting of just one section and the spar was used for the coupled analysis. Figure 5.2 shows the model used. This is a watertight model made such that it is easy to mesh and couple with fluent solver (courtesy: Dr Ming-Chen Hsu).
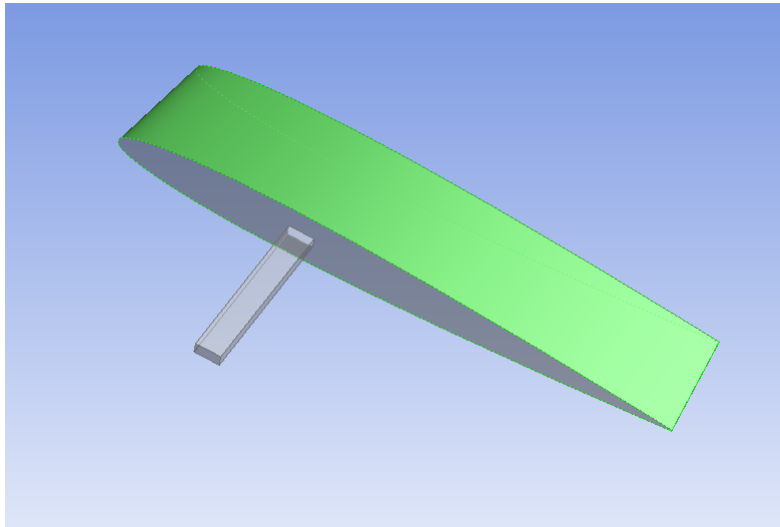

Figure 5.2   Short Model

To set up an interface for transient coupled two way data transfer, system coupling module in the Ansys workbench is used. The two participant solvers in the coupling module are transient structural and fluent. The geometry is shared between the two modules. This '.igs' file is imported to the geometry section of transient structural module. Here we define enclosure used for fluid domain and both-structure and enclosure are separated using Boolean operation. In the transient structural, full integration method is used. Meshing of only structural part is carried out suppressing the fluid domain. Built in features of workbench are used for meshing selecting advanced meshing options on proximity with fine size and medium smoothing.

In the experiment performed in wind tunnel, the initial condition to set the dynamics in motion is given by manual impulse. The same effect is achieved in the simulation model by specifying a non-zero initial condition on the velocity of some of the structural states. Zero free-play condition is modelled by fixed end boundary condition implied on the free end of the spar. Manual damping of 0.25% is applied to the system. All other controls such as nonlinear controls are set as program controlled. For the ease of restart in case of crash/sudden closure, restart options are set to manual and last saved state [Ansys (c), Ansys (d)]. Important step in this module is to define 'Fluid structure Interface'. In this model under consideration, the airfoil surface shown in green color in figure 5.2 is used as Fluid structure interface as the displacement-force two way data transfer is expected at this surface. This surface is again selected in the system coupling module where we define data transfer. This completes transient structural set up.

Using Fluent module in the workbench, first the meshing of fluid domain is completed, by suppressing the structural part. To make this possible, boolean operation is performed to make fluid-structure entities separate yet present under same geometry. Here, built in meshing features are used in fluent keeping advanced meshing on curvature with fine size and medium smoothing. All the regions/domains in the fluid domain such as inlet velocity, outlet pressure, airfoil surfaces etc. are properly named in this step to make the further part easier. Setting up the fluent set-up is important in this coupling [Ansys (a)]. Here all the boundary conditions and dynamic meshing is defined. For faster operations, parallel processing option is selected and since dynamic analysis is performed, it is transient analysis in fluent as well. Pressure

based solver is selected. As per given in the experimental set up, input flow velocity and outlet pressure boundary conditions are set such that experimental conditions are modelled. The structure is fixed at the top and inflow wall is selected in the side of leading edge such that flow is directed perpendicular to the elastic axis as desired. 'No slip wall' boundary condition is set up for airfoil surfaces and other spar faces. Since we require data transfer on fluid structure interface, dynamic meshing is required for such problems. Fluid domain and spar faces are set to deforming dynamic mesh since they will be moving as per the structure's displacement. All the walls of the fluid domain are set to stationery meshing. Importantly, system coupling type dynamic meshing is selected for the airfoil surfaces selected for interface. The mesh on this surfaces will be changed/moved suitable to structure to make data transfer without fail. Also re-meshing and smoothing meshing methods are used since we need mesh to regenerate after each new update in the meshing in the system dynamics. After this, all the reference values, auto-save options and required data output is set up in fluent options. Lift monitors are used to get transient lift values from the system. Also other ASCII files are exported to analyse the data for further energy analysis. Figure 5.3 shows the step by step approach followed in the co-simulation set up.
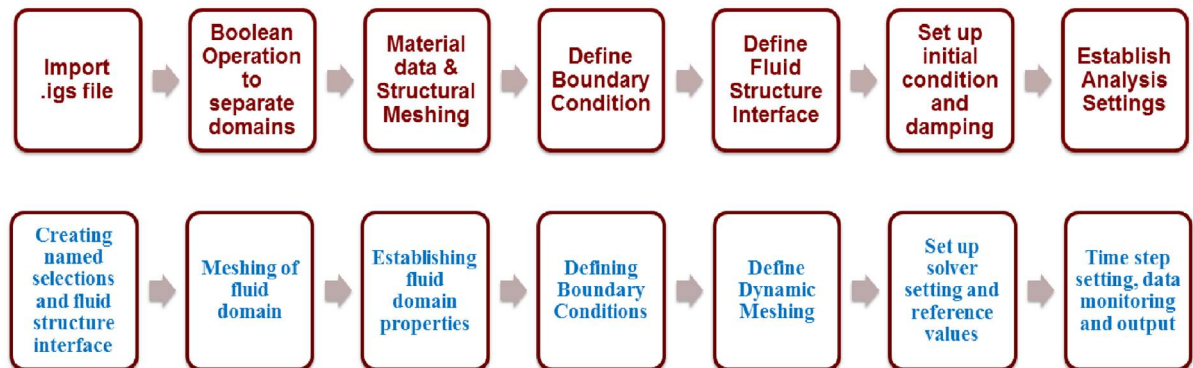

Figure 5.3   Steps in the Workbench set-up

Once the transient and fluent set ups are done, these solvers are to be coupled using system coupling module[Ansys (f)]. As mentioned in previous section, coupling steps and time steps are decided in this module to suit the requirements. Since the FSI is run in the co-simulation, setting up co-simulation sequence is important. Transient structural is the first solver followed by fluent. Another important step is to decide the data transfer between solid and fluid domains. Two way data transfer is established selecting the fluid-structure interface for transient structural and airfoil surfaces for fluent. Displacement and force are corresponding variables selected for data transfer. Source-target relationship is established in each of the two data transfers selected. Load to the structure is transferred from a fluid solver and the deformations to the fluid are transferred from the structural solver. RMS convergence value is kept as 0.01 as default. Figures 5.4 and 5.5 show the data transfer set up in the system coupling module.

Figure 5.4   Data Transfer 1

Figure 5.5   Data Transfer 2

Intermediate restart options are selected as desired in case of sudden simulation crash. Once both solvers are properly connected, the two way coupled system coupling module in Ansys workbench is as shown in figure 5.6
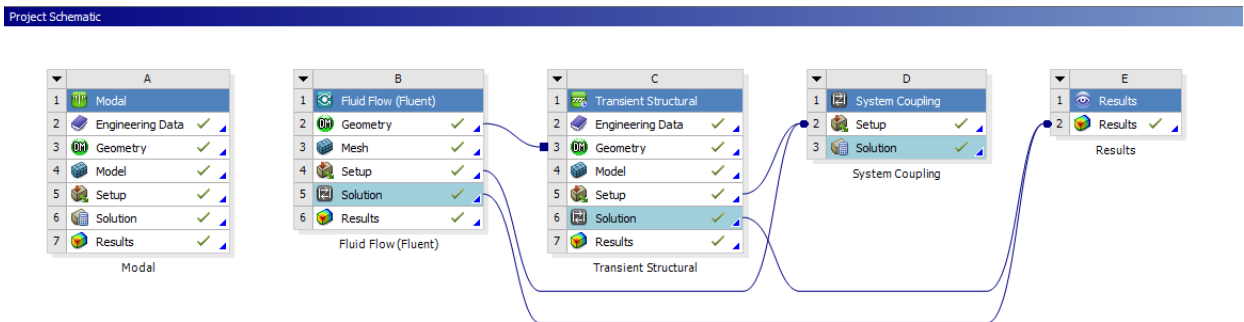

Figure 5.6   Two Way System Coupling Set-up

5.3 Energy analysis of 3D system

Once the system is properly connected, simulation is run for 4 seconds and data is collected to study energy transfer involved in the aeroelastic response.
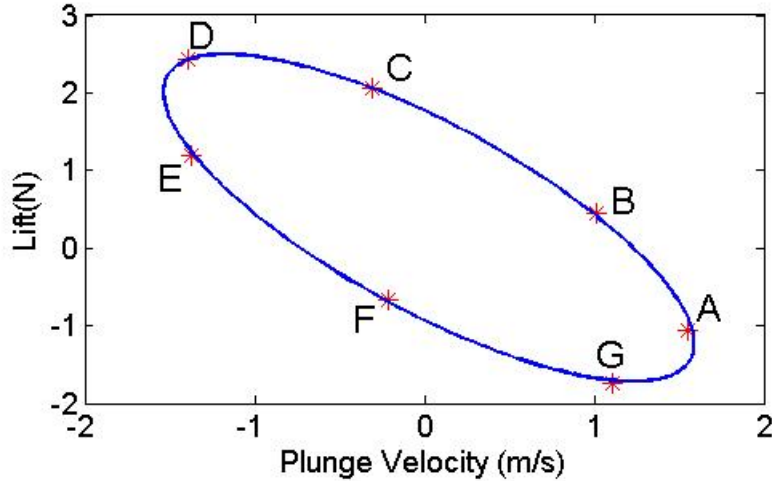

Figure 5.7   Lift vs Plunge Velocity

The study is based on the results obtained from 2D system energy simulations. Similar to the 2D case, kinetic, potential and total energy plots are obtained for the 3D system. As discussed previously, it is important to set the system in the sustained LCO phase. Hence a 3D system is set in the LCO mode by changing the inflow velocity. Since only one section of the entire model is used in the simulation, this LCO onset velocity is found out using trial-error approach such that desired bending-torsion mode is excited and the system is set in sustained LCO after initial nonzero excitation. Also, as we discussed in Chapter 3, the balanced energy transfer sets in between fluid and structure. Figure 5.7 show the elliptical plot (cyclic nature) established between lift and plunge velocity for the 3D system indicating the LCO state.

Some of the results from previous wind tunnel experiment are used to shed light on the energy perspective involved in 3D aeroelastic system. Figure 5.8 shows the FFT results first two mode shapes of the no-free-play model in wind tunnel frequencies migrate together as free stream velocity increases and converges once the flutter velocity is reached.
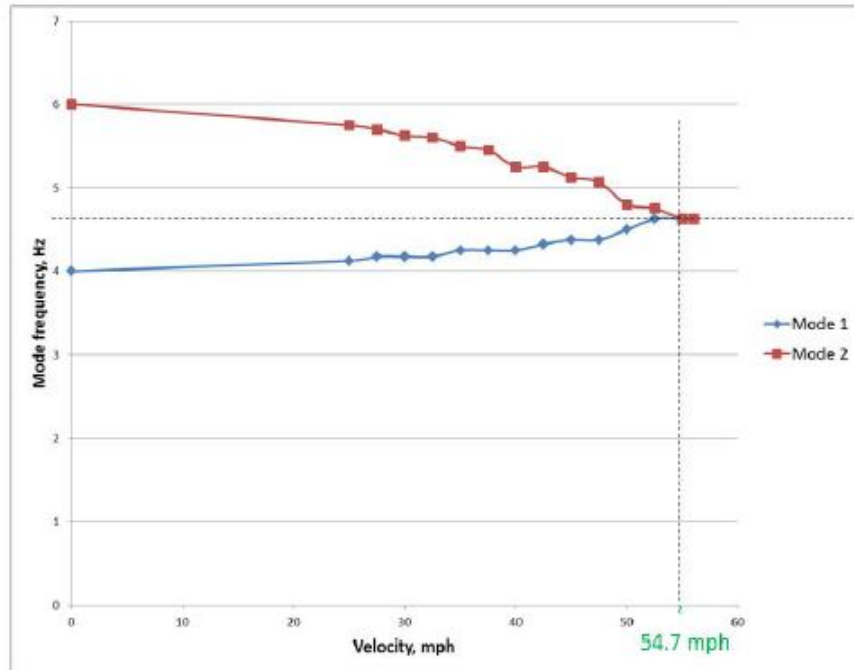
Figure 5.8   FFT Result *

Figures 5.9, 5.10 and 5.11 show system response under different conditions. To analyse the energy perspective in the dynamics of the response all three figures are compared to each other. Figure 5.9 shows the stable damped response of the system. After initial excitation, systems eventually comes to the rest (equilibrium for that stage).

* Courtesy: VSI Aero, Ames, IA

Figure 5.9   Damped Response *

Figure 5.10   Divergent Response *

---

* Courtesy: VSI Aero, Ames, IA

Figure 5.11   Stable LCO Region *

In the damped response shown in figure 5.9, more energy is given back to the fluid than transferred in to the structure. In the divergent case as given in figure 5.10, system shows the unstable divergent response. Here, more energy is pumped into the structure from fluid as compared to structure transferring energy to fluid. Hence total energy going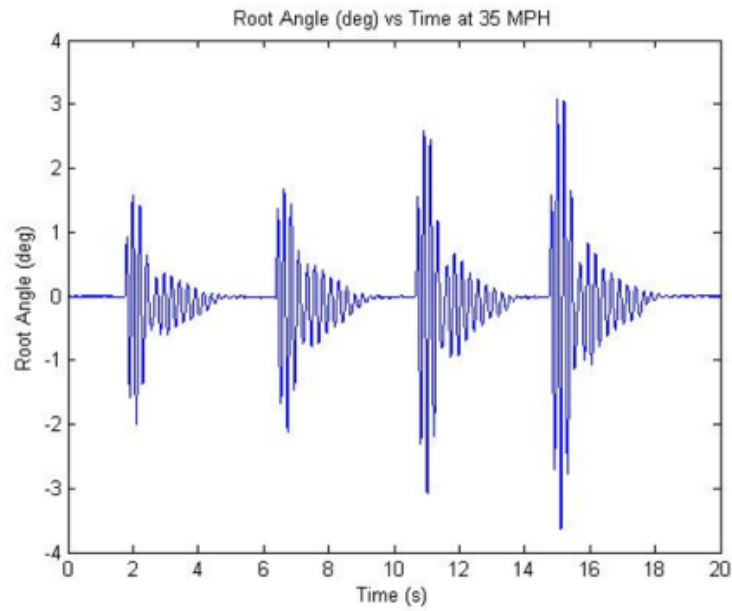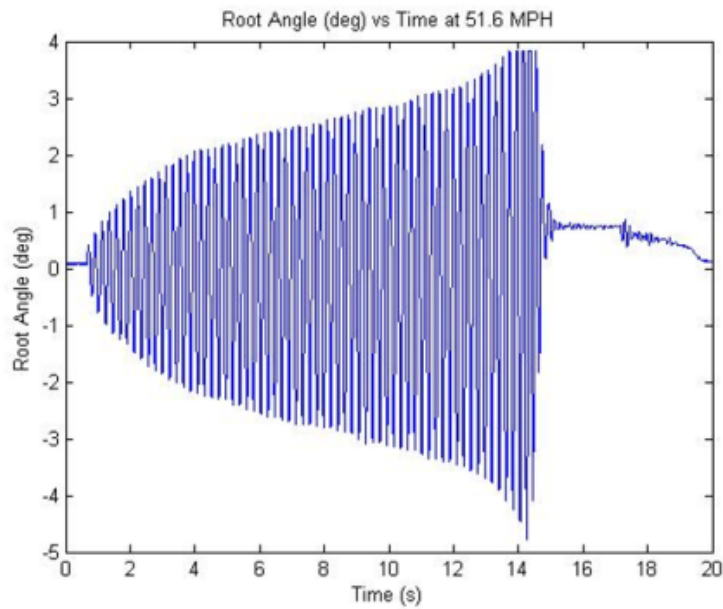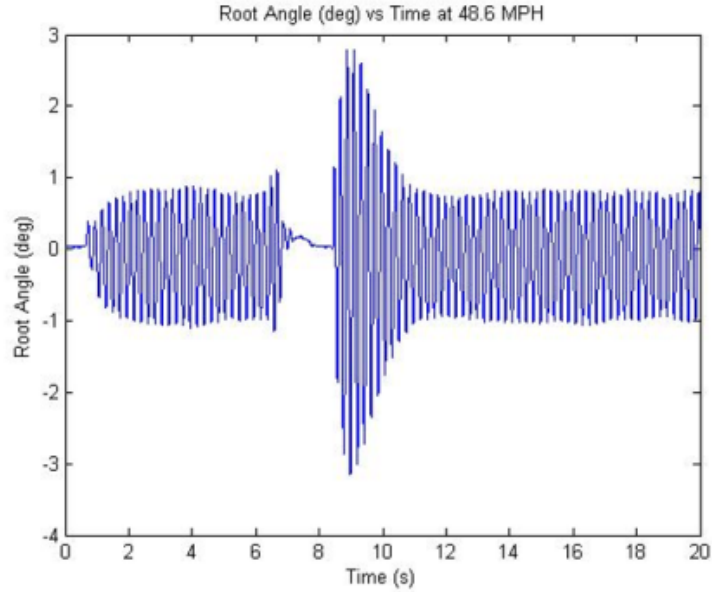 into the system is unbalanced and goes on increasing resulting in the divergent response as shown. This eventually causes the catastrophic failure to the system due to unstable flutter situation. But there exists a wide range of inflow velocities for which system under given conditions establishes stable energy transfer between fluid and structure. This stage is as per given in figure 5.11. It shows sustained, stable LCO set up in the system. As the figure shows for both small and large initial impulses the system eventually settles down to sustained oscillations case. In this case, as discussed in the 2D system, energy balance between fluid and structure is established. Energy given to the fluid from structure is approximately same as energy getting pumped into the structure from fluid.

This energy balanced is captured in the computational model response and it is seen from

---

* Courtesy: VSI Aero, Ames, IA

the cyclic nature of the lift vs plunge velocity plot shown in figure 5.7. Energy variation in each cycle is calculated from the total deformation data obtained from Ansys. The modal analysis is performed for this model to get the mass and stiffness matrices from the Ansys apdl, in order to use for further energy analysis.
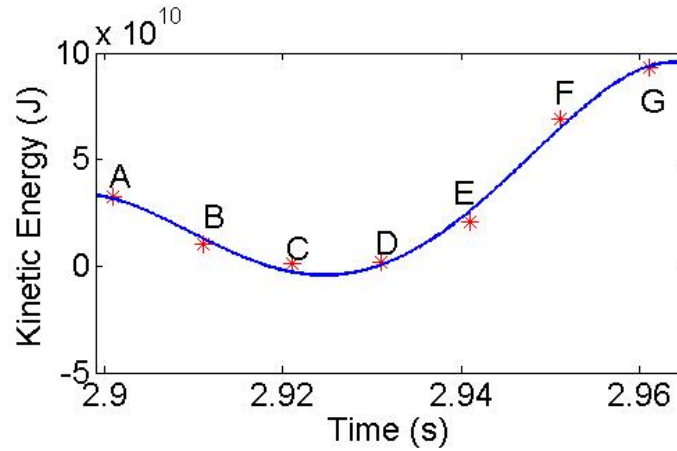

Figure 5.12   Kinetic Energy in one cycle
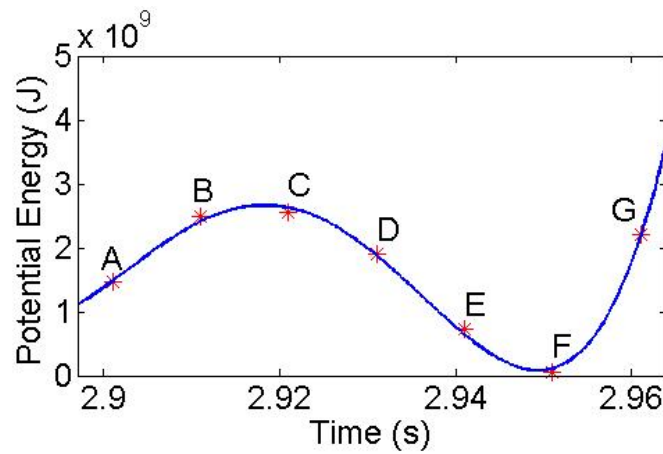

Figure 5.13   Potential Energy in one cycle
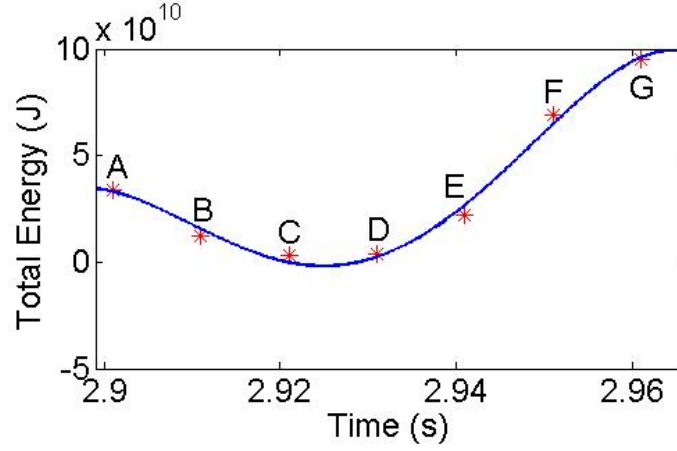
Figure 5.14   Total Energy in one cycle

The matrix files are exported in the standard Harwell-Boeing matrix format. This format consists of row and column indices which can be used to interpret and understand the data given in the column vector format. Matlab is used to convert this format to the standard Matlab sparse matrix format used in further energy calculations. Figures 5.12 and 5.13 shown kinetic and potential energy variation in the system for one cycle.

These energies are calculated as follows:

$$\text{Kinetic Energy} = \frac{1}{2}[\dot{r}]^{\top}[M][\dot{r}] \tag{5.1}$$

$$\text{Potential Energy} = \frac{1}{2}[\dot{r}]^{T}[S][r] \tag{5.2}$$

$$\text{Total Energy} = \text{Kinetic Energy} + \text{Potential Energy} \tag{5.3}$$

Where, [M] and [K] are mass and stiffness matrices and [r] is the deformation vector in 3D. Cyclic nature of the energy are seen as discussed in theoretical 2D case. Also, balance between kinetic and potential energy is also observed. Points A,B,C,D,E can be traced on both energy plots and lift-plunge rate ellipse to get deeper insights into energy analysis. Figure 5.14 shows total energy variation in one cycle. Decrease in total energy of the system shows the energy is transferred from structure to fluid and increase in total energy of the structure shows the energy is pumped from fluid to structure. This interaction is cyclic and balanced as concluded from above figures.

In summary, this chapter presented a detail discussion on setting up the two way coupled simulation for the 3D model. The energy perspective involved in 3D system response is studied based on the representative experimental results and cyclic nature of the energy cycles in computational model. This highlights the proof-of-concept established in the 2D system energy analysis. This study also sheds the light on the exact energy interaction taking place at fluid-structure interface and hence opens up the new potential of energy harvesting possibilities and quantification as discussed in the next chapter.

CHAPTER 6.   ENERGY HARNESSING ANALYSIS

In Chapters 3 and 5, a detail analysis on energy transfer between fluid and structure was studied for 2D and 3D systems respectively. In particular, it was shown that there is a phase of aeroelastic instability wherein the system exhibits sustained (stable) limit cycle oscillations over a range of wind speeds. The oscillation amplitudes vary based on the onset wind speed. This chapter is devoted to the development of concept energy harvesting methodology for harnessing energy from persistent LCO motion of the structure over a range of wind speeds.

6.1   Magnetostrictive Materials

Many smart materials like piezoelectric materials are studied in Erturk et al. (2010), Bryant and Garcia (2011) for harnessing energy involved in vibrations. In recent trends, magnetostrictive materials are also playing important role in energy harvesting applications which is explored in Staley and Flatau (2005), Wang and Yuan (2008), Adly et al. (2010). Magnetostriction is a reversible exchange between the mechanical form and magnetic form. Magnetostrictive materials respond to external stresses by changing its magnetic field and this change in magnetic field induce voltage in the coil. This voltage can further be converted to useful power in other applications. Figure 6.1 shows how rotation and reorientation of small magnetic fields under external magnetic field causes change in length.
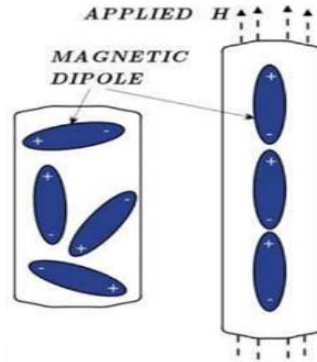
Figure 6.1   Magnetostriction

Two main effects in the magnetostriction are Joule effect and Villari effect as explained in Olabi and Grunwald (2008) and figure 6.2
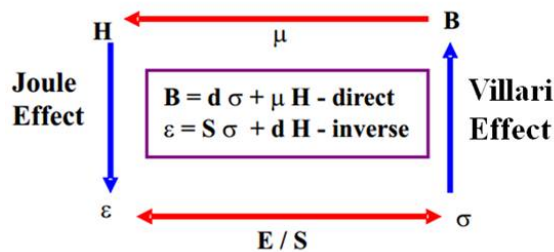
Figure 6.2   Magnetostriction Effects

- Joule Effect: It is the expansion- positive magnetostriction or contraction-negative magnetostriction, of ferromagnetic rod in the longitudinal magnetic field. The change in length causing strain in structure is due to rotation and reorientation of small magnetic domains. In the absence of the magnetic field, the sample shape returns to the original dimensions. This effect is mainly used in magnetostrictive actuators.

- Villari Effect: It is change in the magnetic flux density due to mechanical stresses imposed on the object. In this the mechanical stresses in the object cause the change in magnetic flux density which induces voltage in the coil. It is the open circuit voltage.

Magnetostrictive energy harvesting utilizes the Villari effect. Mechanical stresses due to vibrations are converted into useful electrical energy.

This energy extraction in the flutter response uses Villari effect to harness energy. Mechanism can be developed that induces changing magnetic field, hence the voltage in the coil, due to changing magnetic stresses during bending-torsion mode excited by aeroelastic response.

6.2   Use of Galfenol

Galfenol and Terfenol-D are most used magnetostrictive materials and their properties are studied in Staley and Flatau (2005) and [http://www.etrema.com/galfenol/]. Galfenol is an iron-gallium alloy $(Fe_{100-x}Ga_x)$, x being the variable determined by the desired magnetic properties in the alloy. It is mechanically robust and offers a tensile strength 20 times that of other piezoceramic materials [http://www.etrema.com/galfenol/]. Hence Galfenol can be used for harsh and shock prone applications as well. This gives an edge to the galfenol over other competitive materials. Also it has a good machineability which makes it suitable for conventional machining techniques like forming, threading, rolling, forging and welding making easy integration with new and existing designs. It can be magnetostrictively active even under tension without applying compressive pre-load. It is suitable for wide range of applications involving broadband input energy or varying operating frequencies.Its high curie temperature and less hysterisis losses make it suitable for many application. With all these advantages, galfenol becomes a good selection for application in the harvesting mechanism proposed in this thesis. All the formulae and properties listed in Table 6.1 are referred from Etrema Propriety's published data- Dr. Julie Slaughter (2015) and [http://www.etrema.com/galfenol/]. The set of linear, coupled magnetostrictive equations to be used are as follows:

$$S = s^H T + d_{33} H \tag{6.1}$$

$$B = d_{33}^* T + m u^T H \tag{6.2}$$

where, S is strain, s^H is mechanical compliance (m^2/N) at constant H, H is magnetic field (A/m), T is stress, d_{33} is the magnetostrictive coefficient which is change in strain with magnetic

Table 6.1 List of Galfenol properties

Property	Value
Piezomagnetic Constant, d_{33}	15-30 nm/A
Magnetic permeability, μ	75-100
Desnisty	7800 kg/m^3
Young's Modulus	40-75 GPa
Bulk Modulus	125 GPa
Tensile Strength	350 Mpa

field at constant stress, B is magnetic flux density. d_{33}^* is the inverse magnetostrictive coefficient or change in flux density with stress at constant H, μ^T is the magnetic permeability at constant T.

Equation (6.2) is used for energy harvesting as it relates change in magnetic flux density with changing stress. The changing magnetic flux is converted into useful electric voltage using a wire-wound coil. Voltage induced in the coil is calculated using Faraday's law of induction for a closely wound coil. The generated voltage is given by:

$$V = -NA\frac{dB}{dt} \tag{6.3}$$

where, $\frac{dB}{dt}$ is the change in magnetic flux density with time for a constant cross section and uniform B-field in the centre of the coil. This equation represents open circuit voltage induced by changing magnetic flux and needs additional electrical circuit arrangement to quantify the actual available power output.

Assuming that magnetic field H is constant and substituting for $\frac{dB}{dt}$ the open circuit voltage in galfenol is estimated as:

$$V = -NAd_{33}^*\frac{dT}{dt} \tag{6.4}$$

As seen from the equation, the voltage is related to stress rate. These equations and properties of galfenol listed in Table 6.1 are used in Matlab simulations to calculate the open voltage available due to stress induced in the dynamic aeroelastic response.

6.3   Energy harvesting concept for 2D system

In Chapters 2 and 3, the development and energy analysis is discussed and it is seen that, once the LCO is set, there is a balanced energy transfer between fluid and structure. In 2D system, the free-play nonlinearity is also modelled and it is seen from the previous work that the LCO onset velocity is dependent on the free-play magnitude. Hence, the free-play parameters can be adjusted such that LCO is obtained for changing inflow conditions. This concept is applied in the energy harvesting mechanism. The rotational spring attached to the airfoil is made up of magnetostrictive material galfenol and mechanical strain rates developed in that because of pitching and plunging action are used to induce open circuit voltage.

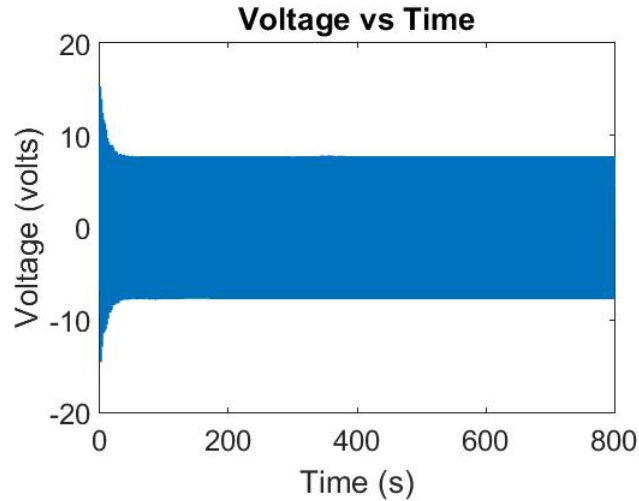Figure 6.3   Induced Voltage

Figures 6.3 and 6.4 show induced voltage using Eq. (6.4). The voltage induced in one cycle shows the cyclic nature due to changing magnetic flux. Voltage induced for the complete simulation time is approximately constant once the LCO is set up after initial non zero condition. Hence energy can be effectively harvested at almost constant rate once the LCO is setup.
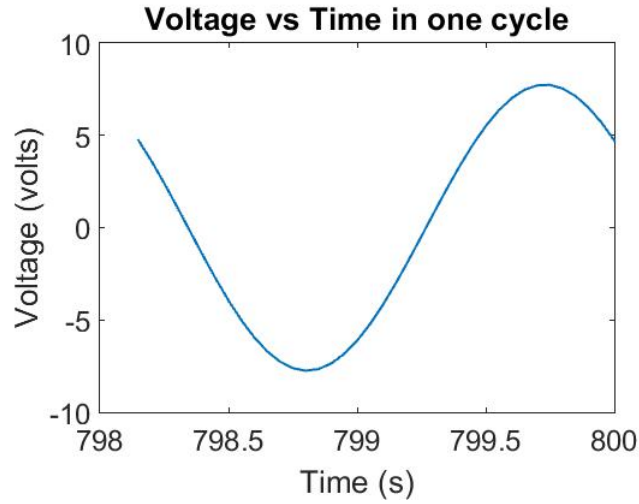
Figure 6.4   Induced voltage in One Cycle

Figure 6.5   LCO after changing δ
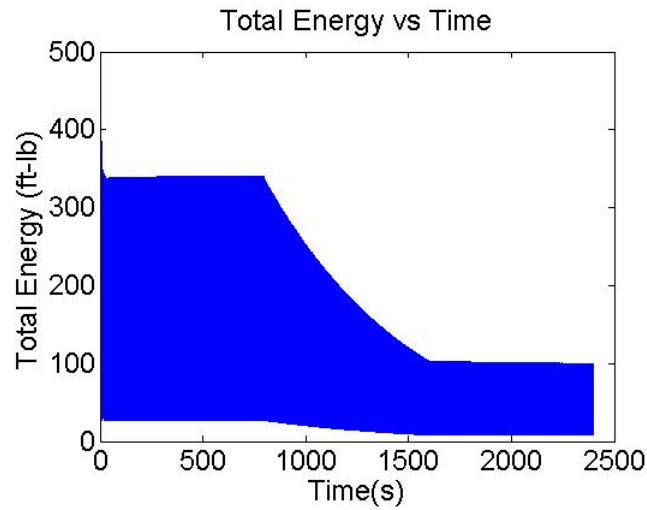
But when energy harvesting process is started, the strain energy available in the structure is decreased. Also, incoming flow velocity can also vary. Hence to make the energy extraction process sustainable, an active control mechanism needs to be developed that can change the free-play nonlinearity parameters and if required K_θ such that LCO is set up at the new flow conditions.

A concept simulation by changing δ for changed inflow velocity is as shown in figure 6.5. This shows that even after change in inflow velocity, nonlinearity parameters can be altered to set the system back into LCO mode with reduced amplitude. Similar changing parameter concept can be applied to reduced magnitude in LCO. Hence, this 2D system analysis for energy harvesting concept is helpful in understanding the road map to develop more efficient and realistic harvesting mechanism for 3D system analysed in the next section.

6.4 Energy harvesting concept for 3D system

The concept of using magnetostriction for energy harnessing can be extended to the 3D system as well. The 3D model under consideration has a spar located at the elastic axis which also acts as rotational axis in this case. The bending-torsion mode excited in the LCO as discussed in the previous chapter generates mechanical strains in this spar. Since magnetostrictive materials have property of converting this stress or strain rate in changing magnetic flux inducing voltage, this spar can be used as a medium generating changing mechanical stresses. This concept is implemented in the model under simulations, and the alternating voltage from the changing magnetic field is obtained for one cycle similar to 2D case. Figure 6.6 shows the open circuit voltage induced in one cycle for 3D system. Since this is just for the one section of the entire model, the concept of magnetostrictive spar can be extended to the complete 3D structure. The concept model, representing magneostrictive spar is as shown in figure 6.7. This spar is subjected to bending-torsion stresses. Since material like Galfenol is machinable and not brittle like other piezo or magnetostrictive materials, it can be potentially used for the construction of the spar which will allow for the optimum energy transfer efficiency.

For the better output, based on wind direction and available space, complete array of this structure can be designed. Figure 6.3 shows the design array concept.
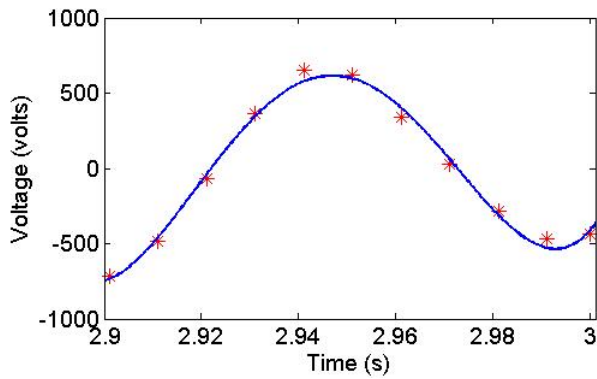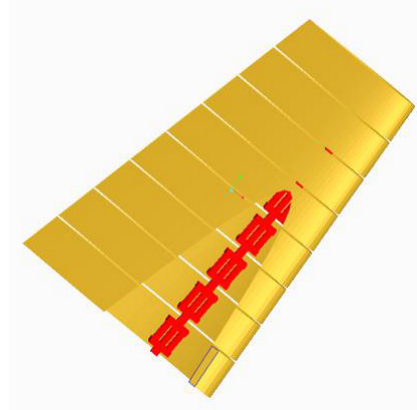
Figure 6.6　Voltage induced in one cycle

Figure 6.7　Design Concept-Galfenol Spar [*]
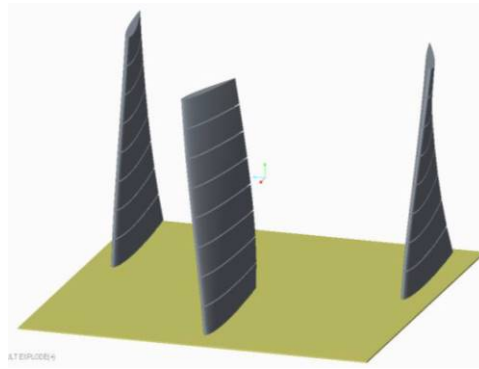
Figure 6.8　Structure Array Concept [*]

A representative conditioning circuit can be designed as shown in the figure 6.9. Its a simple quadruple circuit. The output for the case of structural oscillation frequency considering the stiffer model with higher frequency is as shown in the figure 6.10. A schematic showing a conceptual energy harvesting mechanism is as shown in figure 6.11.

This shows the controller designed to adjust δ and or K_θ based on the free stream velocity and output structural states. Based on the input to the controller, it calculates the free-play magnitude to keep the structure in the sustained oscillation state.Once the structure is set to continuous vibrations, the magnetostrictive spar develops changing magnetic field which is converted to the useful voltage by conditioning circuit which with further modification develops

---

[*]Courtesy: VSI Aero, Ames, IA

electric power.

Figure 6.9   Basic Quadruple Circuit
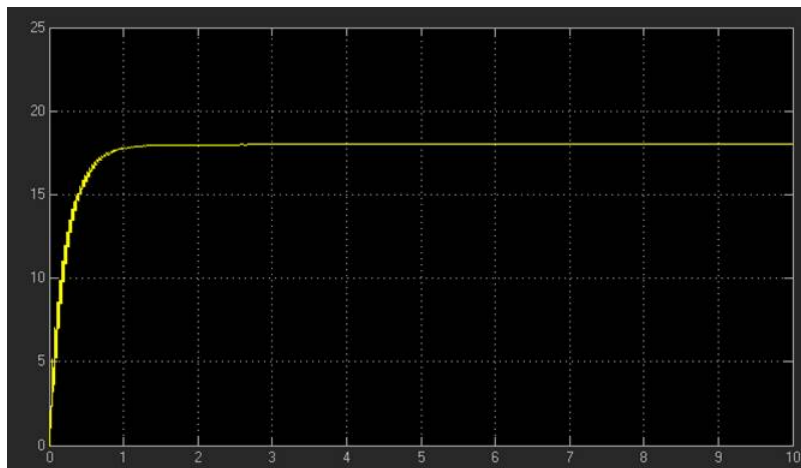
Figure 6.10   Response with higher flutter frequency
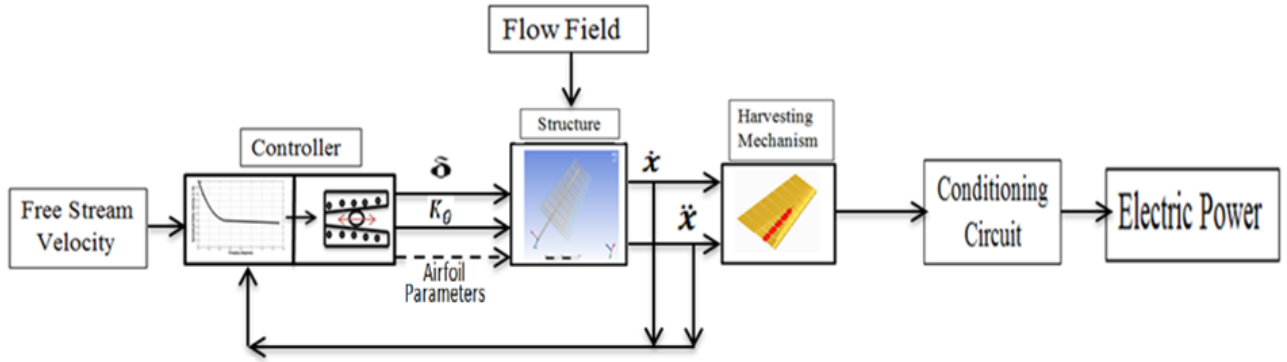
Figure 6.11   Energy harvesting schematic block diagram
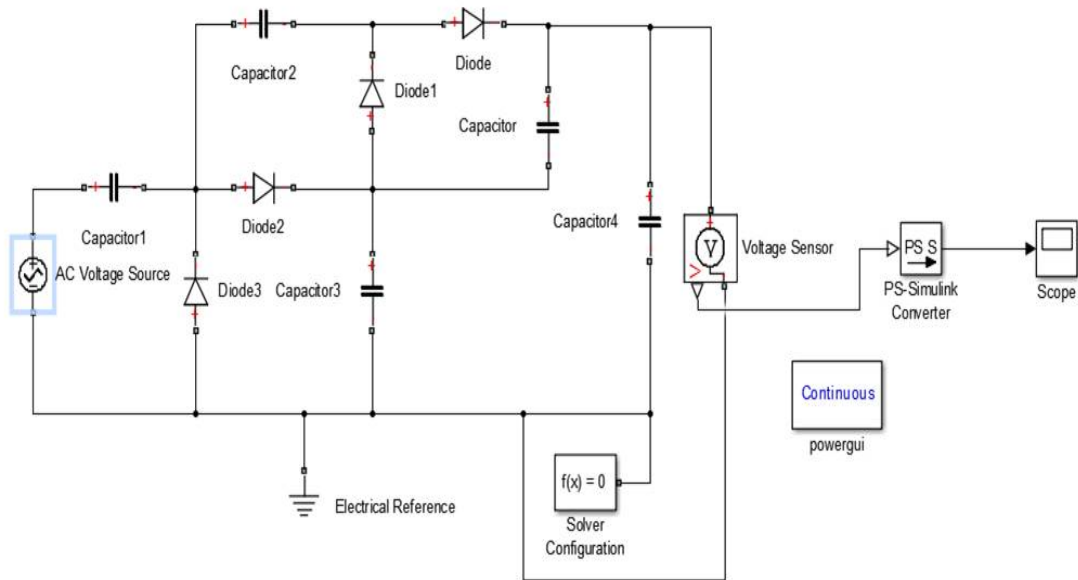
The figure also shows the future concept of changing airfoil parameters for the better output. Hence properly designed controller can lead to the effective and efficient energy harvesting from aeroelastic system dynamics.

6.5   Key benefits of proposed concept

Following are the important benefits of this proposed harvesting mechanism

- The concept uses wind as an input energy which is a clean and renewable source of energy

- It uses solid state material for energy conversion which causes less losses in energy conversion and gives better conversion efficiency

- To the best of current knowledge, there is no theoretical limit on energy output possible from this mechanism. All the electrical and mechanical losses can be tackled with better design strategies.

- This design avoids use of big gearboxes causing less mechanical losses

- The design is compact, robust and do not require huge foundation structures. It can be successfully erected on the building roofs and grounds.

- Proper controller design enables better and efficient energy output.

CHAPTER 7. CONCLUDING REMARKS AND FUTURE WORK

The main objective of this work was to understand the energy transfer involved in aeroe-lastic fluid structure interaction and exploit the dependence of marginally stable oscillations of aeroelastic structure on the free-play for energy harvesting. The 2D and 3D systems were anal-ysed to study LCO behaviour and energy interaction in sustained oscillations. As a first step, a proof of concept 2D model was used for detail analysis to characterize the energy exchange involved and to validate the experimental findings from previous wind tunnel tests. The 2D model analysis demonstrated mathematically the anticipated phenomena that the sustained energy transfer takes place between fluid and structure during during LCO motion and it can be used for harnessing energy. Having demonstrated successfully in 2D case, the modelling and analysis effort was extended to a more realistic 3D configuration. A high fidelity computa-tional model was developed using a well known commercial package, Ansys, for analysing energy transfer phenomenon in 3D. Due to this computational power and time limitations, without loss of generality, a reduced order model with only one airfoil section was used to conduct com-putational studies. In the case of 3D model it was assumed that the spar of the model is built using Galfenol. Analysis similar to 2D case was conducted to successfully demonstrate that the same phenomena (physics) is observed in the 3D case as well. A concept energy harvesting mechanism and associated control strategy was also discussed. The electrical throughput was simulated using this methodology for a reduced order 3D system. Given below is the summary of the key contributions of this work.

7.1   Key Contributions:

- Analytical study of energy transfer and energy harvesting in 2D aeroelastic system with free-play nonlinearity:

  Although there exists abundance of literature on modeling and analysis of 2D aeroelastic system with nonlinearity in joint stiffness there does not exist any study that explores the aeroelastic dynamics from energy viewpoint. This work gives a deeper understanding of what is happening in the energy domain as the aeroelastic system moves through different phases of motion. Having understood the energy exchange during aeroelastic instability a concept energy harvesting methodology was also proposed and demonstrated in simulation using 2D system.

- Energy analysis of 3D aeroelastic model response in different stability regions and harvesting methodology:

  The work presented here on energy analysis for a fully coupled 3D aeroelastic system is a unique contribution. The work demonstrated conceptually intuitive and logical phenomena of energy exchange between structure and flow field using higher fidelity computational model resembling real physical system. The results from 3D simulations showed that the 2D analysis directly extends to 3D case. Moreover, the work also presented some practical design concepts for energy harvesting mechanism using the ideas proposed in this work.

- Methodology for using magnetostriction to harness energy in the proposed aeroelastic system: The work presented here discussed the rationale for the choice of specific magnetostrictive material, Galfenol, in comparison to other available choices. A detail mathematical study was also presented to compute the electrical throughput that can be generated in both 2D and 3D example cases to demonstrate the efficacy of the proposed harvesting methodology.

In summary, the work in this thesis is expected to be foundational for the concept of recovering energy in the flow field through a free-play induced LCO instability. Further work by researchers

is anticipated to evaluate economic viability, mechanical strength issues and exploring potential technical and economical limitations of the concept. Given below are suggestions for future work in this area.

7.2   Future Work

The future work needed to realize the energy harvesting concept outlined in this thesis is given below:

- Extending the computational study from a scaled 3D model to a full scale 3D model.

- Development of a spar design that is machinable using Galfenol and assessing its fatigue life.

- Design of an efficient electric circuitry to avoid minimum energy loss in harvesting.

- Full scale wind tunnel testing of the concept and assessing economic and technical viability

- Developing concept of a bank of airfoils that can provide energy harvesting over a very wide range of wind speeds.

BIBLIOGRAPHY

Adly, A., Davino, D., Giustiniani, A., and Visone, C. (2010). Experimental tests of a magnetostrictive energy harvesting device toward its modeling. *Journal of Applied Physics*, 107(9):09A935.

Ansys. *Ansys Fluent Users Guide*. Ansys Inc.

Ansys. *Ansys Mechanical APDL Structural Analysis Guide*. Ansys Inc.

Ansys. *Ansys Mechanical Users Guide*. Ansys Inc.

Ansys. *Ansys Structural Analysis Guide*. Ansys Inc.

Ansys. *Guide to Interfacing with Ansys*. Ansys Inc.

Ansys. *System Coupling Users Guide*. Ansys Inc.

Asjes, D. (2015). *Thesis*. PhD thesis, Iowa State University.

Asjes, D., Diwadkar, A., Vaidya, U., Kelkar, A., Vogel, J. M., and Chaussee, D. (2014). Modeling and analysis of rotational freeplay nonlinearity of a 2d airfoil. In *American Control Conference (ACC), 2014*, pages 1162–1167. IEEE.

Bennett, R. M. and Edwards, J. W. (1998). An overview of recent developments in computational aeroelasticity. *AIAA paper*, 2421.

Bryant, M. and Garcia, E. (2011). Modeling and testing of a novel aeroelastic flutter energy harvester. *Journal of vibration and acoustics*, 133(1):011010.

De-Min, Z. and Qi-Chang, Z. (2010). Bifurcation and chaos analysis for aeroelastic airfoil with freeplay structural nonlinearity in pitch. *Chinese physics B*, 19(3):030518.

Dr. Julie Slaughter, E. S. (2015). *Galfenol Energy Harvesting.* Etrema Products, Inc.

Earl H. Dowell, Edward F. Crawley, H. C. C. J. D. A. . P. R. H. S. and Sisto, F. (1995). *A Modern Course in Aeroelasticity.*

Edwards, J. W. and Wieseman, C. D. (2008). Flutter and divergence analysis using the generalized aeroelastic analysis method. *Journal of Aircraft*, 45(3):906–915.

Erturk, A., Vieira, W., De Marqui Jr, C., and Inman, D. (2010). On the energy harvesting potential of piezoaeroelastic systems. *Applied Physics Letters*, 96(18):184103.

Gupta, K. (1996). Development of a finite element aeroelastic analysis capability. *Journal of Aircraft*, 33(5):995–1002.

Hoffman, N. R. and Spielberg, I. N. (1954). Subsonic flutter tests of an unswept all-movable horizontal tail. no. wadc-tr-54-53. *WRIGHT AIR DEVELOPMENT CENTER WRIGHT-PATTERSON AFB OH.*

Kim, T., Hong, M., Bhatia, K. G., and Sengupta, G. (2005). Aeroelastic model reduction for affordable computational fluid dynamics-based flutter analysis. *AIAA journal*, 43(12):2487–2495.

Ko, J., Kurdila, A. J., and Strganac, T. W. (1997). Nonlinear control of a prototypical wing section with torsional nonlinearity. *Journal of Guidance, Control, and Dynamics*, 20(6):1181–1189.

Ko, J., Strganac, T. W., and Kurdila, A. J. (1998). Stability and control of a structurally nonlinear aeroelastic system. *Journal of Guidance, Control, and Dynamics*, 21(5):718–725.

Lee, B., Gong, L., and Wong, Y. (1997). Analysis and computation of nonlinear dynamic response of a two-degree-of-freedom system and its application in aeroelasticity. *Journal of Fluids and Structures*, 11(3):225–246.

Lee, B., Price, S., and Wong, Y. (1999). Nonlinear aeroelastic analysis of airfoils: bifurcation and chaos. *Progress in aerospace sciences*, 35(3):205–334.

Mukhopadhyay, V. (2003). Historical perspective on analysis and control of aeroelastic responses. *Journal of Guidance, Control, and Dynamics*, 26(5):673–684.

Northington, J. S. (2009). Basis vector quantification of flutter analysis structural modes. *Journal of Aircraft*, 46(6):2107–2114.

Olabi, A.-G. and Grunwald, A. (2008). Design and application of magnetostrictive materials. *Materials & Design*, 29(2):469–483.

Park, J.-K., Kim, K.-M., Kwon, S.-D., and Law, K. H. (2012). An aero-elastic flutter based electromagnetic energy harvester with wind speed augmenting funnel. *Online http://eil. stanford. edu/publications/jinkyoo_park/AWAS12. pdf.*

Patil, M. J. (2002). Limit cycle oscillations of aircraft due to flutter-induced drag. In *Proceedings of the 43rd Structures, Structural Dynamics and Materials Conference, Denver Colorado.*

Patil, M. J. (2003). From fluttering wings to flapping flight: The energy connection. *Journal of Aircraft*, 40(2):270–276.

Silva, W. A. and Bartels, R. E. (2004). Development of reduced-order models for aeroelastic analysis and flutter prediction using the cfl3dv6. 0 code. *Journal of Fluids and Structures*, 19(6):729–745.

Sousa, V., de M Anicézio, M., De Marqui Jr, C., and Erturk, A. (2011). Enhanced aeroelastic energy harvesting by exploiting combined nonlinearities: theory and experiment. *Smart Materials and structures*, 20(9):094007.

Staley, M. E. and Flatau, A. B. (2005). Characterization of energy harvesting potential of terfenol-d and galfenol. In *Smart Structures and Materials*, pages 630–640. International Society for Optics and Photonics.

Strganac, T. W. et al. (2012). Aeroelastic response of a rigid wing supported by nonlinear springs. *Journal of Aircraft.*

Tang, D. and Dowell, E. H. (2006). Flutter and limit-cycle oscillations for a wing-store model with freeplay. *Journal of Aircraft*, 43(2):487–503.

Theodorsen, T. (1949). General theory of aerodynamic instability and the mechanism of flutter.

Trickey, S., Virgin, L., and Dowell, E. (2002). The stability of limit–cycle oscillations in a nonlinear aeroelastic system. In *Proceedings of the Royal Society of London A: Mathematical, Physical and Engineering Sciences*, volume 458, pages 2203–2226. The Royal Society.

Trickey, S. T. (2000). *Global and local dynamics of an aeroelastic system with a control surface freeplay nonlinearity.*

Wang, L. and Yuan, F. (2008). Vibration energy harvesting by magnetostrictive material. *Smart Materials and Structures*, 17(4):045009.

Whitmer, C., Kelkar, A. G., Vogel, J. M., Chaussee, D., Ford, C., and Vaidya, U. (2012). Modeling and characterization of the impact of control surface free-play on flutter for an all moving surface. In *American Control Conference (ACC), 2012*, pages 5342–5347. IEEE.